ACS chemical biology

pubs.acs.org/acschemicalbiology

Articles

Designer Small-Molecule Control System Based on Minocycline-Induced Disruption of Protein−Protein Interaction

Ram Jha, Alexander Kinna, Alastair Hotblack, Reyisa Bughda, Anna Bulek, Isaac Gannon, Tudor Ilca, Christopher Allen, Katarina Lamb, Abigail Dolor, Ian Scott, Farhaan Parekh, James Sillibourne, Shaun Cordoba, Shimobi Onuoha, Simon Thomas, Mathieu Ferrari, and Martin Pule*

Cite This: ACS Chem. Biol. 2024, 19, 308−324

Read Online

ACCESS | Metrics & More | Article Recommendations | Supporting Information

ABSTRACT: A versatile, safe, and effective small-molecule control system is highly desirable for clinical cell therapy applications. Therefore, we developed a two-component small-molecule control system based on the disruption of protein−protein interactions using minocycline, an FDA-approved antibiotic with wide availability, excellent biodistribution, and low toxicity. The system comprises an anti-minocycline single-domain antibody (sdAb) and a minocycline-displaceable cyclic peptide. Here, we show how this versatile system can be applied to OFF-switch split CAR systems (MinoCAR) and universal CAR adaptors (MinoUniCAR) with reversible, transient, and dose-dependent suppression; to a tunable T cell activation module based on MyD88/CD40 signaling; to a controllable cellular payload secretion system based on IL12 KDEL retention; and as a cell/cell inducible junction. This work represents an important step forward in the development of a remote-controlled system to precisely control the timing, intensity, and safety of therapeutic interventions.

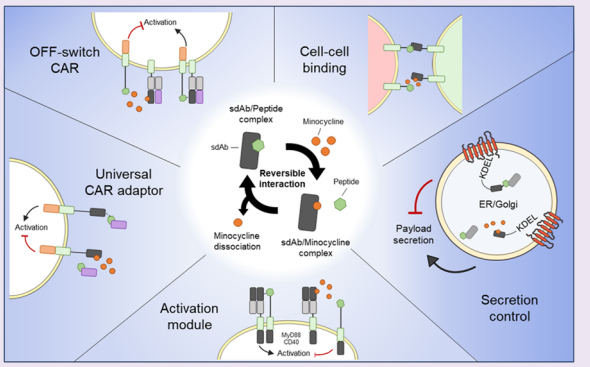

INTRODUCTION

Engineered cellular therapies have emerged as a promising approach for treating a wide range of diseases including cancer, autoimmune disorders, and genetic diseases. Unlike small molecules or protein therapeutics, however, many cellular therapies engraft in patients and may persist and expand in an autonomous fashion. Consequently, therapeutic activity cannot be easily titrated with dose, and toxicities can be progressive and fulminant. Hence, the means of controlling the activity of cellular therapies remotely, for instance, through administration of small molecules is desirable.

Several small-molecule cellular control systems have been developed: the best characterized exploit Rapamycin's ability to complex simultaneously with FKBP12 and the FRB fragment of mTOR/FRAP.[1] Heterodimerization of proteins fused to FKBP12 and FRB can be induced by Rapamycin. Alternatively, homodimerization can be induced in FKBP12 fusion proteins by AP1903, a homodimer analogue of Tacrolimus. This system has been used to generate suicide genes,[2,3] inducible antigen receptors,[4−6] and inducible cytokine receptors.[7] Analogous strategies using other small-molecule-mediated homo/heterodimerization have been described.[8]

A different strategy to control protein−protein interaction exploits proteases that can be controlled by small-molecule protease inhibitors: in one example, two protein domains are separated by a herpes C virus (HCV) protease cleavage. The two protein domains are cleaved by a coexpressed HCV protease; however, in the presence of a cognate protease inhibitor, cleavage is inhibited, and hence the two protein domains do not associate.[9,10]

Alternatively, engineered protein−protein interactions can be disrupted upon exposure to a small molecule. Such systems may be more clinically convenient since a small molecule would only need to be administered in the case of toxicity. One such system was described by Giordano-Attianese et al., where the Bcl-XL and Bcl-2 homology 3 (BH3) domain of BIM were used as the heterodimerization drivers of protein−protein interaction, prevented by two clinically tested Bcl-2 inhibitors.[11] We previously described an analogous approach: by fusing one protein to a tetracycline mimicking peptide (TiP), and a second protein fused to TetRB, exposure to tetracycline can disrupt TiP/TetRB interaction.[12]

While there are a number of small-molecule control systems, many of these systems are limited by immunogenicity (HCV, TetRB), lack of availability of the small molecule (AP1903 and

Received: August 24, 2023
Revised: January 1, 2024
Accepted: January 4, 2024
Published: January 20, 2024

https://doi.org/10.1021/acschembio.3c00521
ACS Chem. Biol. 2024, 19, 308−324

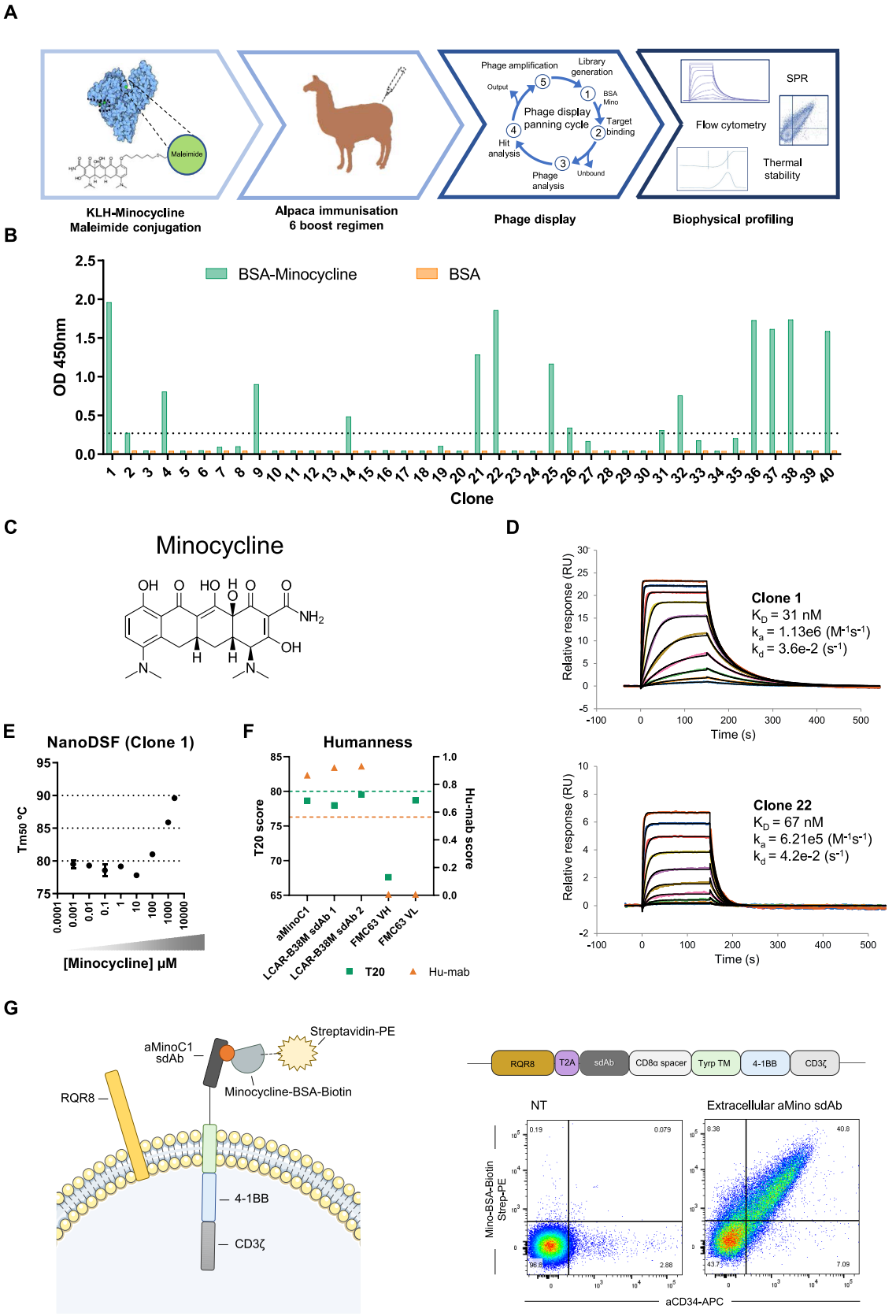

Figure 1. Generation and biophysical characterization of an anti-minocycline sdAb. (A) Schematic of immunization strategy, phage display selection, and biophysical characterization of anti-minocycline sdAb. (B) ELISA screen of monoclonal anti-minocycline sdAb clones. Screening of purified monoclonal sdAb was carried out against BSA-conjugated minocycline. Fourteen clones showed positive binding to minocycline and a lack of binding to BSA alone control (OD > 6× baseline). (C) Minocycline chemical structure. (D) Surface plasmon resonance (SPR) of anti-minocycline sdAb-Fc clone 1 (aMinoC1) (top) and clone 22 (aMinoC22) (bottom) binding to minocycline. aMinoC1 and aMinoC22 presented KD values of 31 and 67 nM, respectively. (E) Analysis of sdAb stability by nanoDSF. Thermal unfolding temperature (Tm) of aMinoC1 in the

https://doi.org/10.1021/acschembio.3c00521
ACS Chem. Biol. 2024, 19, 308−324

Figure 1. continued

presence of its binding partner at concentrations from 1 nM to 1 mM. Protein concentration of 1 mg mL^{-1} suspended in PBS pH 7.4. (F) T20 score (green) and Hu-mab score (orange) analysis of aMinoC1 sdAb in relation to LCAR-B38M sdAbs (Ciltacabtagene autoleucel)[73] and FMC63 VH and VL domains. Dashed lines indicate threshold of human-like sequences for respective scoring. (G) Schematic representation of the aMinoC1 transmembrane receptor (aMinoC1-CD8stk-TyrpTM-41BBz) and RQR8 transduction marker (left). Flow cytometry dot plot of transduced HEK-293T cell surface expression for RQR8 (anti-CD34) and aMinoC1 receptor (minocycline−BSA−biotin). Linear correlation of expression between the aMinoC1 receptor and the RQR8 marker on the cell surface.

nonimmunosuppressive rapalogs),[11,13,14] and unwanted pharmacologic activity of the inducing small molecule (Rapamycin). Additionally, with increasingly complex cellular engineering approaches, multiple orthogonal controls may be desired.

Here, we sought to develop a new small-molecule control system. We selected minocycline as the ideal inducer as it is a widely used antibiotic with few pharmacological side-effects. To avoid immunogenicity, often associated with xenogeneic proteins, we based the system on a minocycline-recognizing single-domain antibody (sdAb) sharing high homology with the human VH3 family. We additionally identified a cyclic peptide that competed with minocycline for sdAb binding to result in a protein−protein interaction control system disrupted by minocycline. We tested several applications based on these two protein domains with the control affected by minocycline-induced disruption of protein−protein interactions.

RESULTS

Generation of Minocycline-Specific Single-Domain Antibodies via Phage Display. Minocycline-specific single-domain antibodies were generated by the immunization of a single alpaca with KLH-conjugated minocycline and subsequent phage display panning (Figures 1A and S1). Seroconversion was first confirmed by ELISA (Figure S2A), and after two rounds of phage panning, enrichment was observed (Figure S2B).

Over 40 sdAbs from pan 2 were screened, and among the 14 clones showing specific binding to minocycline (Figure 1B), 9 unique sequences were identified (Figure S2C,D). aMinoC1 showed the strongest interaction with minocycline, with an SPR-determined KD of 31.6 nM (Figure 1C). This interaction was confirmed by isothermal titration calorimetry (ITC), showing a KD of 24.9 (±5.59) nM (Figure S3A). aMinoC22 showed a KD of 67 nM (Figure 1C). Neither sdAb showed an interaction with the closely related molecules doxycycline and tetracycline (Figure S3B).

The conformational stability of the high-affinity sdAb antibody in complex with minocycline was investigated using nano differential scanning fluorimetry (nanoDSF). aMinoC1 showed high thermal stability with the first unfolding midpoint (Tm_{50}) of 79.5 °C. Coincubation with minocycline ranging from 1 nM to 2.5 mM improved the Tm_{50} values by over 10 °C, increasing to 89.6 °C, indicating an antigen-driven stabilizing event (Figure 1E). *In silico* analysis of aMinoC1 indicated a high humanness score, suggesting limited immunogenicity (Hu-mAb score 0.875[15] and T20 score 78.66[16]) (Figure 1F). Finally, the ability of aMinoC1 to be expressed on the surface of a cell and bind minocycline was shown by expressing this sdAb in a type I surface protein format and staining with labeled minocycline (Figure 1G).

Generation of a Displaceable Cyclic Peptide. We next sought to identify a peptide that would compete for aMinoC1 sdAb binding. A combinatorial phagemid library of cysteine-constrained 7-mer peptides (CX_7C) was enriched via phage display for aMinoC1 sdAb binders. Isolated monoclonal phagemids were examined by ELISA to determine their binding to sdAb and displacement by minocycline. Seventeen out of 20 selected monoclonal phage clones showed specific binding to aMinoC1 with reduction of binding when co-incubated with 1 μM minocycline (Figure 2A). Sequencing the peptide coding region of phagemids indicated a homologous consensus motif (Pro-X-Trp-Ala-X-X-Phe) and a total of four unique peptide sequences with amino acid differences at positions X2, X5, and X6 (Figure 2B).

The measured affinities (KD) of GWARA, HWAQA, PWAYS, and QWAMM peptides were 111, 328, 283, and 209 nM, respectively, with varying kinetic profiles, with the former showing the highest affinity and the fastest on-rate (Figure S3C). Specific binding of the peptides to aMinoC1 sdAb and competition with minocycline were confirmed by ELISA as purified peptide-Fc conjugates. All peptides showed significant displacement from aMinoC1 sdAb in the presence of minocycline, while no binding was detected for the nonrelated sdAb clone 31 (Figure 2C).

Reversible association and dissociation of the peptides were then demonstrated using a modified SPR protocol. Peptide binding to immobilized aMinoC1 (phase I) was specifically reversed by the addition of minocycline (phase II) and not by two closely related small molecules (doxycycline and tetracycline). Removal of the drug (phase III) then allowed subsequent rebinding of the peptide to a comparable degree to that before, confirming the sustained structural integrity of the aMinoC1 binding pocket. Serial binding/dissociation cycles confirmed robust reversibility of the system (Figures 2D and S4).

Minocycline was able to elicit a concentration-dependent reduction in peptide binding, for all four CX_7C constructs tested, in the context of a membrane-bound aMinoC1 sdAb architecture. Additionally, incubation with 100 μM caffeine did not result in a decrease in peptide binding (Figure 2E).

Understanding the Minocycline and Peptide-Binding Interface on sdAb. We sought to understand the molecular interactions between aMinoC1 sdAb and both minocycline and the GWARA peptide. Crystallography failed due to the low resolution of crystal formation. We subsequently performed an alanine scan, mutating all three CDR regions of the antibody and determined the effect on minocycline affinity by SPR (Figure 3A). Mutagenesis identified a predominant role for the CDR3 region (positions 110−112 and 115−117), with additional contact points in positions 38 and 55 of CDR1 and CDR2 in binding to minocycline. Effects of alanine scanning on GWARA-peptide binding were assessed by ELISA. In contrast to minocycline binding, this identified positions 28, 35, and 40 of CDR1, positions 58, 63, and 64 of CDR2, and position 108 of CDR3 as the main drivers of peptide binding (Figure 3B), suggesting a stronger role for CDRs 1 and 2.

https://doi.org/10.1021/acschembio.3c00521
ACS Chem. Biol. 2024, 19, 308−324

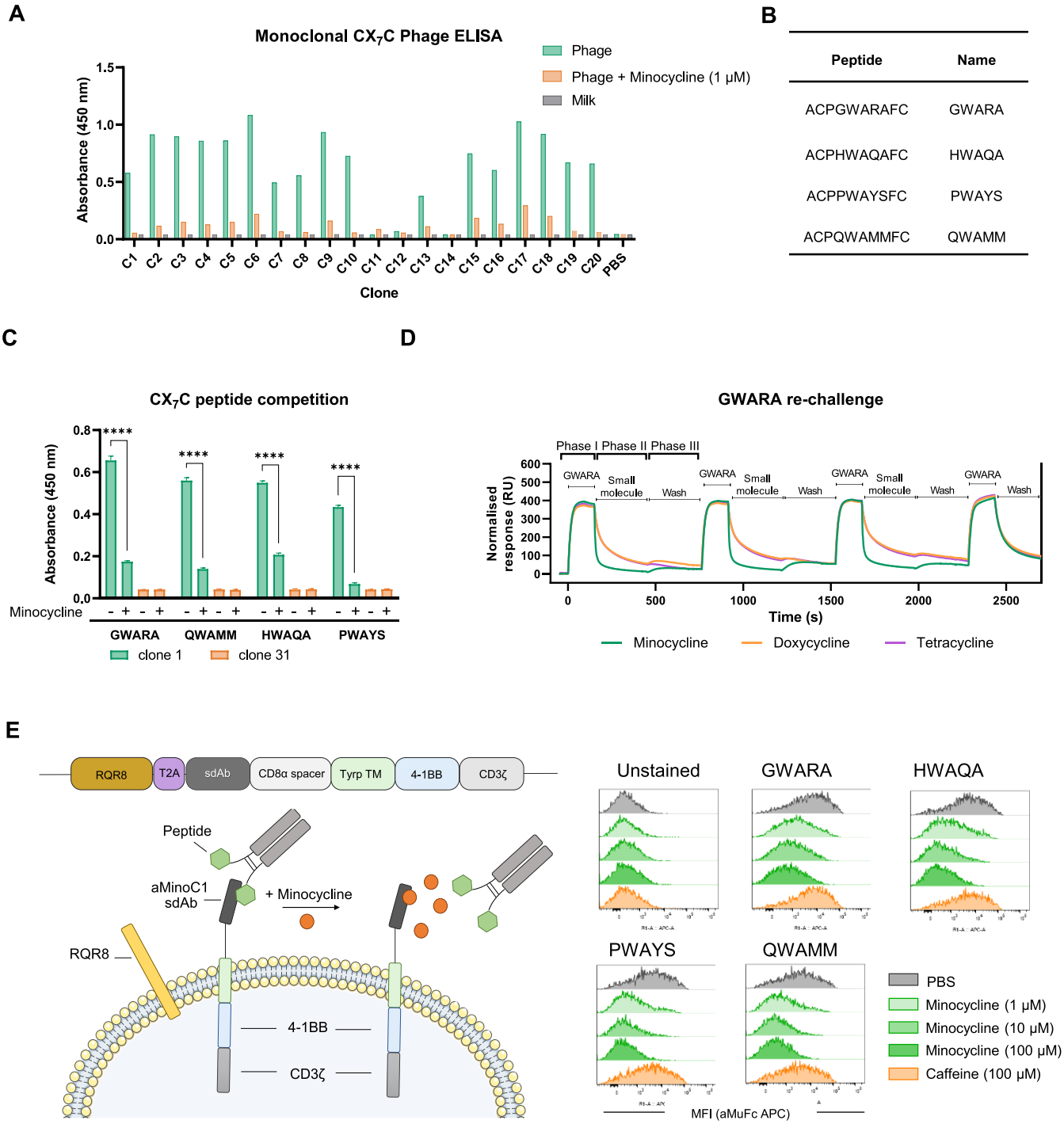

Figure 2. Engineering of a minocycline-displaceable CX7C peptide with affinity for aMinoC1 sdAb. (A) Anti-M13 detection ELISA of selected monoclonal whole phagemid clones displaying CX_7C peptides binding to plate-immobilized aMinoC1 sdAb with or without minocycline (1 μM). (B) Four unique peptide sequences (GWARA, HWAQA, PWAYS, and QWAMM) were isolated and tested for sdAb binding as peptide-muIgG2a-Fc conjugates. (C) ELISA of purified CX_7C-muIgG2a-Fc peptide fusion showing specific binding to aMinoC1 sdAb. Addition of 1 μM minocycline out-competed peptide-Fc conjugates resulting in significantly reduced detection. Two-way ANOVA with Sidak's post-test. ****$P < 0.0001$. (D) Dynamic minocycline (green), doxycycline (orange), or tetracycline (purple) small molecules and GWARA-peptide-Fc binding to immobilized aMinoC1 sdAb on Biacore 8k. Sequential injections of GWARA-Fc (Phase I), small molecule (Phase II), and dissociation (buffer, wash) step (Phase III) showing minocycline-driven acceleration of GWARA-Fc dissociation. Serial challenges with peptide and small molecule show reversibility of the system. No enhanced dissociation was visible with doxycycline or tetracycline injections. (E) Schematic representation of cells expressing RQR8 transduction marker and aMinoC1 transmembrane receptor detected with peptide-muIgG2a Fc in the presence of minocycline (left). Histogram plot of flow cytometry staining for HEK-293T transduced with the aMinoC1 transmembrane receptor, with peptide-muIgG2a Fc peptide fusion (right). Dose-dependent reduction of peptide-muIgG2a Fc binding for GWARA, HWAQA, PWAYS. and QWAMM in the presence of increasing concentrations of minocycline (green gradient). 100 μM caffeine incubation (orange) showed no peptide-binding inhibition compared to the PBS control condition (gray).

https://doi.org/10.1021/acschembio.3c00521
ACS Chem. Biol. 2024, 19, 308−324

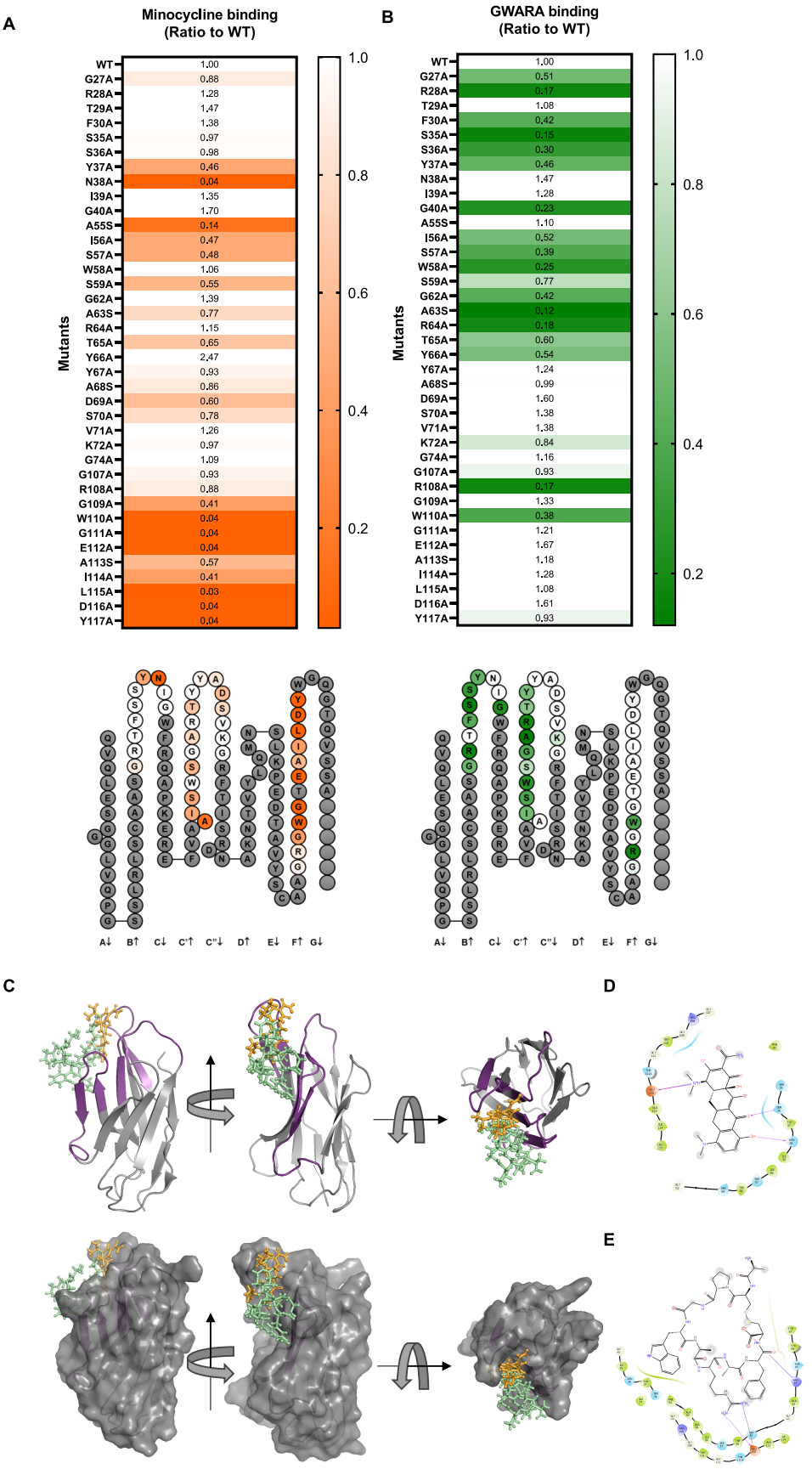

Figure 3. Minocycline and GWARA-peptide-binding interface for aMinoC1. Alanine scanning was performed on IMGT and Kabat-defined CDR regions to maximize the areas of interest: CDR1 positions from 27 to 40, CDR2 from 55 to 74, and CDR3 from 107 to 117. Where present, Ala residues were mutated to Serine. (A) (top) Ratio of minocycline binding kinetics (KD) of wild-type (wt) aMinoC1 and alanine-scan variants (color scale range 0.03−1.0), measured by SPR. Color scale: white for no change (1.0 ratio), dark orange for low binding of variant compared to wt (0.03

https://doi.org/10.1021/acschembio.3c00521
ACS Chem. Biol. 2024, 19, 308−324

Figure 3. continued

ratio). (bottom) Collier de Perles representation of critical amino acid residues (no change: white, lower affinity: orange). Nonmutated residues are shown in gray. (B) (top) Ratio of binding of wt aMinoC1 and alanine-scan variants to GWARA-Fc peptide by ELISA (color scale range 0.12−1.0). Color scale: white for no change (ratio 1.0), dark green for low binding of variant compared to wt (ratio 0.12). (bottom) Collier de Perles representation of critical amino acid residues (no change: white, lower affinity: green). Nonmutated residues are shown in gray. (C) Superimposed computational antibody−ligand docking of aMinoC1 with minocycline (orange) and GWARA peptide (green) showing a cartoon display (CDR in purple) structure (top) and surface display (bottom) for aMinoC1. (D) Interaction diagram for aMinoC1 and minocycline. (E) Interaction diagram for aMinoC1 and GWARA peptide.

Experimental data suggested a disparity of putative contact interactions between antibody/minocycline and antibody/peptide complexes. To determine if a spatial clash was likely to drive minocycline−peptide competition, we performed computational docking simulations against a 3D model of aMinoC1 using previously defined rotamer conformations for the ligands (Figure S5). Top ranking poses indicated the colocalization of both ligands within the same groove of the antibody (Figure 3C−E). Despite the limitations of *in silico* modeling, data suggest that steric hindrance is likely to be the main driver of minocycline/peptide competition. Notably, the predicted MHC-I immunogenicity of MinoCAR was low in comparison with widely used clinical components[17,18] (Figure S6).

Development and In Vitro Testing of a Novel OFF-Switch CAR T Cell. We first explored the use of this system to generate a controllable CAR. A bipartite CAR architecture (MinoCAR) was constructed, consisting of separate antigen recognition and signaling components. The antigen recognition component was composed of a two-arm Fab structure with an anti-EGFR sdAb arm and the aMinoC1 sdAb fused to the transmembrane and endodomain of CD28. The T cell signaling component comprised the GWARA peptide on an extracellular spacer connected to the intracellular 41BB and CD3ζ signaling domains. We hypothesized that in the absence of minocycline, these components associate, allowing the CAR to signal in response to antigen, while minocycline would cause dissociation and CAR inhibition (Figure 4A).

The cytotoxicity, cytokine release, tunability, and reversibility of MinoCAR were tested against both engineered and endogenous EGFR positive cell lines (SupT1 and SKOV3, respectively) (Figure S7A,B). At 24 and 72 h, without minocycline, cytotoxicity toward SupT1-EGFR$^+$ target cells was observed, equivalent to a control conventional monolithic EGFR CAR (Figure 4B). Cocultures in the presence of minocycline demonstrated a dose-dependent reduction in cytotoxicity and significantly increased target cell survival (average 2.5- and 35-fold increase at 24 and 72 h, respectively, compared to 0 μM minocycline condition). Similarly, IFN-γ and IL2 secretion levels in the absence of minocycline were comparable to the conventional EGFR CAR, while minocycline supplementation significantly reduced cytokine secretion (minus 2.7- and 1.9-fold for IFN-γ and IL2, respectively) (Figure 4C). Notably, MinoCAR was not affected by small-molecule analogues doxycycline and tetracycline or other small molecules such as methotrexate or caffeine (Figure S7C).

MinoCAR is Tunable and Can Be Reversibly Controlled. Tunability of MinoCAR was tested by measuring the kinetics of cytolysis when exposed to a range of minocycline concentrations. In the absence of minocycline, the rate and extent of cytotoxicity displayed by MinoCAR were comparable to the monolithic EGFR CAR, while increasing concentrations of minocycline induced a dose-dependent decrease in SKOV3 target cell killing (Figure 4D). Next, we sought to investigate the ability of MinoCAR T cells to recover activity following inhibition with minocycline or, conversely, the ability of the drug to inhibit MinoCAR T cells following their activation through exposure to tumor. MinoCAR T cells were subjected to either EGFR-induced activation (activated) or minocycline-mediated inactivation (inhibited). These pretreated cells were then recovered, washed, and cultured with target cells in the presence or absence of minocycline (Figure 4E) and their cytotoxicity compared to cells that had not received pretreatment (either inhibition or activation). MinoCAR T cells without pretreatment displayed cytotoxicity in the absence of minocycline and were inhibited by the drug's presence, as expected. Preactivated CAR T cells displayed the expected cytotoxicity in the absence of the drug but were rapidly inhibited by minocycline and displayed little to no cytotoxicity, indicating that activated cells could be quickly and thoroughly inhibited by exposure to minocycline and displayed little to no residual activity. Conversely, preinhibited CAR T cells quickly recovered activity once the drug was removed, displaying kinetics of target cell killing similar to the "no pretreatment" condition (Figure 4E). These results demonstrate that both activation and inhibition of MinoCAR T cells are rapidly reversible.

In a NOD scid γ (NSG) Nalm6 EGFR$^+$ tumor mouse model, PBMCs transduced with MinoCAR showed significant tumor burden control, comparable to the conventional aEGFR CAR. Mice treated with minocycline showed a significantly reduced MinoCAR efficacy, similar to the effect of a nonfunctioning CAR (Figures 4F and S7D).

sdAb-Peptide Engager-Mediated Redirecting of Cytotoxic T Cells. The use of soluble universal receptor engager proteins to direct cytotoxic T cells engineered with a universal CAR has been previously suggested as a therapeutic strategy.[19,20] We sought to explore whether aMinoC1/GWARA could be used to constitute a universal CAR system with additional minocycline control. We hence developed a two-component universal CAR system (MinoUniCAR) consisting of a universal acceptor CAR component comprising the aMinoC1 binding domain and a soluble functionalizing moiety consisting of a tumor-target binding domain carrying the GWARA-peptide tag (Figure 5A). As a proof of concept, we selected anti-EGFR sdAb as the tumor-targeting adaptor and fused it to the GWARA-peptide tag.

To test the MinoUniCAR system, the EGFR-peptide adaptor protein was added exogenously to CAR-transduced PBMCs at a concentration that was previously determined to provide efficient CAR activation (Figure S8). MinoUniCAR stimulated by EGFR antigen on plate-bound assays showed efficient IFN-γ release, which was rapidly inhibited in the presence of minocycline with a 10-fold cytokine reduction (148 vs 1569 pg/mL for 10 and 0 μM minocycline, respectively) (Figure 5B). Similarly, minocycline was able to

https://doi.org/10.1021/acschembio.3c00521
ACS Chem. Biol. 2024, 19, 308−324

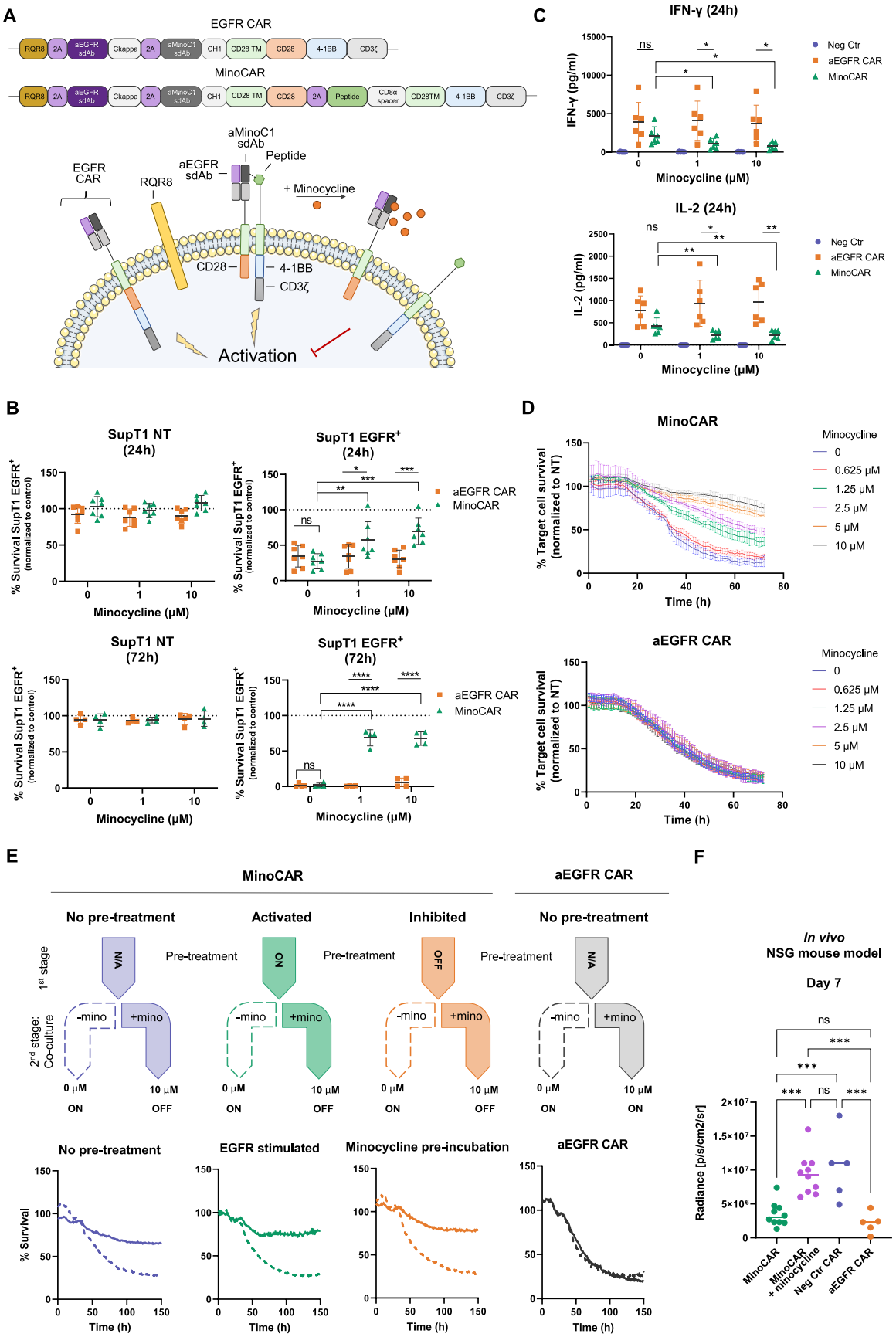

Figure 4. Functional characterization of an OFF-switch CAR T cell (MinoCAR). (A) Schematic representation of monolithic aEGFR Fab-like CAR (EGFR/aMinoC1 sdAb-CD28TM-CD28−4−1BBz) and of split MinoCAR (EGFR/aMinoC1 sdAbs-CD28TM-CD28) with GWARA signaling module (peptide-CD28TM-4−1BBz). GWARA/aMinoC1 binding inhibited by the addition of minocycline. (B) Cellular cytotoxicity for PBMC transduced with monolithic aEGFR CAR (orange) and MinoCAR (green) against SupT1-NT (left) and SupT1-EGFR$^+$ (right) at 24 (top, *n*

https://doi.org/10.1021/acschembio.3c00521
ACS Chem. Biol. 2024, 19, 308−324

Figure 4. continued

= 7) and 72 h (bottom, n = 4), 1:2 E/T ratio. Cocultures incubated with minocycline at 0, 1, or 10 μM. % survival normalized against negative control MinoCAR carrying an irrelevant peptide (SG_3S). Mean ± SD, two-way ANOVA with Sidak's or Tukey's post-test, *P < 0.05, **P < 0.01, ***P < 0.001, ****P < 0.0001. (C) INF-γ (top) and IL2 (bottom) cytokine secretion from PBMCs transduced with aEGFR CAR (orange) or aMinoC1 CAR (green) against SupT1-EGFR$^+$ target cells (n = 6), 1:2 E/T ratio, 24 h. Negative control MinoCAR (blue) carried an irrelevant SG_3S peptide. Mean ± SD, two-way ANOVA with Dunnett's post-test, *P < 0.05, **P < 0.01. (D) Kinetics of cytotoxicity of SKOV3 EGFR$^+$ target cells cocultured with PBMCs transduced with MinoCAR (green) or aEGFR CAR (orange). Mean ± SD, n = 3, 1:2 E/T. Minocycline incubated at a range of concentrations from 0 to 10 μM. (E) Kinetics of cytotoxicity of SKOV3 EGFR$^+$ mKate$^+$ cocultured with PBMCs transduced with MinoCAR (left) or aEGFR CAR (right). MinoCAR PBMCs were subjected to no pretreatment (blue), plate-based EGFR stimulation (green), or minocycline incubation (orange). Cells were further incubated with target cells in the presence of 0 μM (dashed arrow) or 10 μM (solid arrow) minocycline. The presence of minocycline in the second-stage treatment caused inhibition of MinoCAR killing capacity (bottom, solid line) compared to the absence of treatment (bottom, dashed line). % survival normalized against NT PBMCs. Mean ± SD, n = 3, 1:2 E/T ratio. (F) BLI readout at day 7 post CAR-T injection in a NSG Nalm6 EGFR$^+$ tumor mouse model. Significant inhibition of MinoCAR with minocycline injection. One-way ANOVA with Tukey's post-test, ***P < 0.001, ns = not significant.

inhibit the MinoUniCAR cytotoxicity when cocultured against target SupT1-EGFR$^+$ cells, with on average 95% cell survival. In the absence of the drug, MinoUniCAR recovered cytotoxic capacity. The control EGFR CAR was not affected by minocycline (Figure 5B).

Minocycline-Mediated Control of Cellular Signaling. We next tested whether aMinoC1-GWARA engagement could be harnessed to control cellular signal transmission. As a proof of concept, we sought to test a construct that can transmit tunable MyD88/CD40 signals. A MyD88/CD40-inducible system using multimerization induced by FKBP12/AP1097 has been previously described by Foster et al.[21] and was found to have application in CAR T cell therapy. We generated a dual aMinoC1 Fab architecture fused to an IgG1 hinge, CD28TM and MyD88/CD40 endodomains, paired with a GWARA peptide on a CD8stk with CD28TM and MyD88/CD40 endodomains (Figure 5C). A version including a SG_3S peptide instead of GWARA was used as a negative control. In the absence of additional stimuli, transduced PBMCs with the aMinoC1/GWARA-MyD88/CD40 module showed significantly higher IFN-γ secretion (520 vs 218 pg/mL of negative control), a response that was tuned down by an average of 2-fold, with increasing concentrations of minocycline (Figure 5D).

Minocycline-Mediated Secretion of an Antitumor Payload. We next investigated whether the minocycline control system could be used to control protein secretion. We hypothesized that fusing the Lys−Asp−Glu−Leu (KDEL) motif with aMinoC1 could promote its retention in the Golgi. Hence, a GWARA-peptide-tagged secreted protein would be constitutively directed to the Golgi, while minocycline-mediated dissociation from aMinoC1/KDEL would allow its secretion.

We used IL12 to test this system. IL12 can potently activate immune responses against cancer but has a narrow therapeutic window with toxicity occurring even when secreted by engineered immune cells. A single chain variant of IL12 (p35 linked to p40, flexi-IL12)[22] was functionalized with the GWARA peptide (GWARA-flexi-IL12) and expressed alongside aMinoC1 carrying the KDEL retention motif at the C-terminal (Figure 5E). Control constructs consisted of GWARA-flexi-IL12 alone or coexpressed with the aMinoC1 sdAb lacking the KDEL motif to prevent retention.

Transduced T cells were monitored at 2- and 7-days post-transduction for cumulative IL12 secretion in the presence of minocycline ranging from 0 to 2.5 μM. ELISA data showed efficient secretion of control GWARA-flexi-IL12 at days 2 and 7 without modulation induced by minocycline (Figure 5F). The presence of aMinoC1 without KDEL retention caused lower secretory capacity, probably ascribable to a larger transcriptional and translational burden, but similarly unaffected by the presence of minocycline. The GWARA-flexi-IL12 with aMinoC1-KDEL showed no detectable IL12 at day 2 and only 450 pg/mL at day 7. Incremental addition of minocycline triggered a dose-dependent release of IL12 up to 150 pg/mL on day 2 and 2.2 μg/mL on day 7 (Figure 5F).

sdAb-Peptide Engagement as Cellular Organizers. We hypothesized that the aMinoC1/GWARA interaction could also be used to trigger selective cell−cell interactions and formation of organized cellular aggregates. The suspension cell line SupT1 was engineered to coexpress membrane-bound GWARA and mCherry. A second set of SupT1 cells were instead engineered to coexpress membrane-bound aMinoC1 and eGFP (Figure S9). Coculture of the two cell lines with 10 μM minocycline showed a random distribution of cells without a clear spatial organization. However, in the absence of minocycline, a time-course observation of cells in culture showed the rapid formation of cellular aggregates indicating dynamic cooperation of GWARA and aMinoC1 SupT1 cells (Figures 5G,H, S9 and Supplementary Video 1).

DISCUSSION

Increasingly complex cell-based therapies are being used to treat a range of diseases. Examples include engineered immune cells to treat cancer and autoimmunity,[23,24] engineered hematopoietic stem cells to treat monogenic disorders,[25] and therapies with iPS-derived cells applied to degenerative diseases.[26] However, unlike small molecule or protein-based therapeutics, cellular therapies may engraft, expand, and function in an autonomous fashion. Consequently, therapeutic potency or toxicity cannot easily be controlled by stopping administration or titrating dose. Toxicity can therefore be fulminant and uncontrollable.[27] Control systems that can modulate the activity of engineered cells in response to small-molecule pharmaceuticals have been described. These allow "remote control" of cellular therapies and can ensure safety and modulate activity.

Initial control systems exploited the ability of small molecules to induce protein−protein interaction. The earliest designs of such "ON systems" exploited Rapamycin-mediated heterodimerization of FKBP12 and the FRB fragment of mTOR.[1,28,29] Wu et al. designed a Rapamycin-controllable CAR by incorporating FKBP12 and FRB components into split antigen recognition and signaling components.[4] Variations of this approach have also been described where FRB and

https://doi.org/10.1021/acschembio.3c00521
ACS Chem. Biol. 2024, 19, 308−324

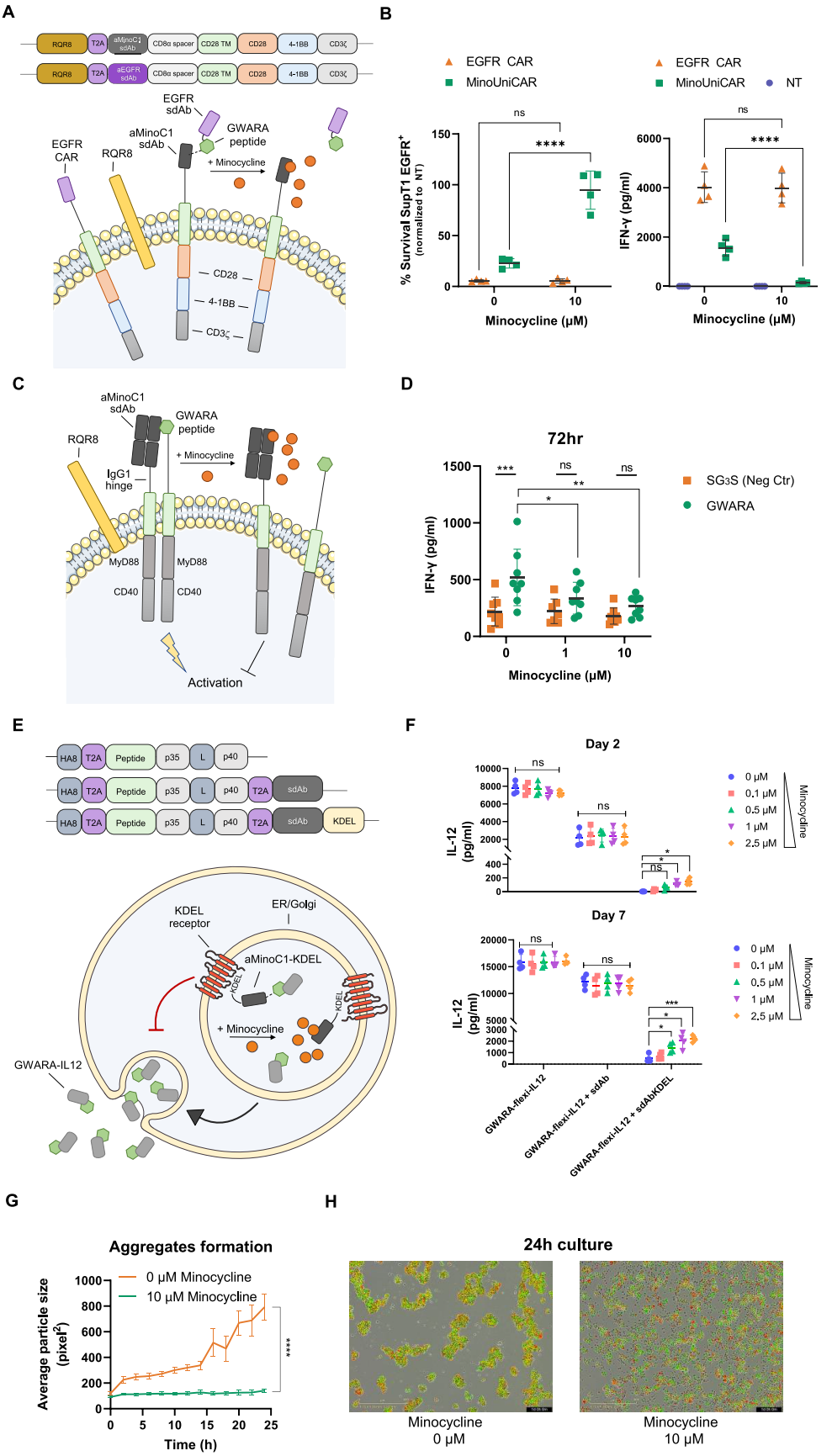

Figure 5. Extended applications for minocycline-tunable control module. (A) Schematic overview and construct design for aEGFR CAR (aEGFR sdAb-CD8stk-CD28TM-CD28-41BBz), universal adapter CAR MinoUniCAR (aMinoC1-CD8stk-CD28TM-CD28-41BBz), and soluble aEGFR sdAb-GWARA functionalizing molecule. (B) Cytotoxicity (left) and IFN-γ secretion (right) for transduced PBMC with test CAR constructs (in panel A) cocultured with SupT1-EGFR$^+$ target cells. % target cell survival normalized to NT PBMCs. Minocycline incubated at 0 or 10 μM for 24

https://doi.org/10.1021/acschembio.3c00521
ACS Chem. Biol. 2024, 19, 308−324

Figure 5. continued

h, 1:2 E/T ratio, $n = 4$. Significant increase in target cell survival and decreased IFN-γ secretion in the presence of minocycline. Two-way ANOVA with Sidak's post-test, ****$P < 0.0001$. NT = nontransduced. (C) Schematic representation of controlled signaling module based on MyD88/CD40 endodomains. Construct includes aMinoC1 Fab-like CAR-IgG1 hinge spacer-CD28TM-MyD88-CD40. A separate polypeptide carries the GWARA-peptide-CD8stk-CD28TM-MyD88-CD40. Addition of minocycline can dissociate aMinoC1-GWARA binding and prevent signaling. (D) IFN-γ secretion by PBMCs transduced with aMinoC1-MyD88-CD40 construct with GWARA-MyD88/CD40 (green) or control SG_3S-MyD88/CD40 (orange) constructs. The absence of minocycline showed significant upregulation of IFN-γ by GWARA-MyD88/CD40 compared to SG_3G-MyD88/CD40. Dose-dependent decrease of IFN-γ secretion visible at increasing concentrations of minocycline. $n = 8$, 72 h. Two-way ANOVA with Sikak's post-test, *$P < 0.05$, **$P < 0.01$, ***$P < 0.001$. (E) Schematic of ER/Golgi retention system for minocycline-mediated secretion of GWARA-tagged flexi-IL12 by aMinoC1-KDEL. Control molecules include untagged aMinoC1 and no aMinoC1. (F) Minocycline-induced secretion of GWARA-flexi-IL12 from transduced PBMCs on anti-CD3/anti-CD28 plate-based stimulation. Significant dose-dependent GWARA-flexi-IL12 secretion at days 2 and 7 for aMinoC1-KDEL in the presence of minocycline concentrations from 0 to 2.5 μM ($n = 4$). Two-way ANOVA with Dunnett's post-test, *$P < 0.05$, ***$P < 0.001$. (G) Time-course cell aggregation formation for SupT1 cells transduced with GWARA-CD8stk-CD28TM and mCherry, cocultured with SupT1 cells transduced with aMinoC1-CD8stk-CD28TM and eGFP in the presence of 0 (orange) or 10 μM (green) minocycline ($n = 3$). Two-way ANOVA for the main effect model, ****$P < 0.0001$. (H) Representative snapshot of cocultures at 24 h with 0 μM (top) or 10 μM (bottom) minocycline for SupT1 GWARA-CD8stk-CD28TM and mCherry (red) and aMinoC1-CD8stk-CD28TM and eGFP (green). Colocalization of the signal is visible in yellow.

FKBP12 components are extracellular[6] and where FKBP12-FRB interactions control CAR immune synapse length to tune activity.[5] Additional examples of FKRBP12/FRB use include suicide genes where Rapamycin induces Caspase 9 activation.[3] However, Rapamycin is immunosuppressive and nephrotoxic,[30] which is a limitation for many applications. To address this, pharmacologically inert "bumped" Rapamycin analogies such as AP21967 have been developed that interact with FRB mutated with complementary "holes", but not with wild-type FRB.[31]

Alternative control systems that also use small molecules to induce protein−protein interaction have been described. These take advantage of the pharmacological inhibitors of viral proteases. In one example, an inducible CAR is designed such that a linker recognized by a hepatitis C protease connects the antigen recognition and signaling domains of the receptor (SNIP-CAR). The protease is coexpressed, resulting in constitutive cleavage with separation of antigen recognition and signaling domains and hence CAR inactivation; small-molecule inhibitors of the protease such as grazoprevir and ritonavir prevent this separation, rendering the CAR active.[9]

Alternatively, small-molecule control systems can be engineered to disrupt the protein−protein interaction (OFF systems). The first example of this was described by Giordano-Attianese et al.[11] Here, the interaction between mitochondrial protein Bcl-XL and the BH3 domain of BIM was targeted. The authors engineered a human scaffold (LD3) derived from apolipoprotein 4, with the BH3 motif. The Bcl-XL/LD3 complex could then be displaced by two existing Bcl inhibitors, A1331852 and A1155463. Incorporation of the two components into a split CAR resulted in the ability to control CAR activity with the Bcl inhibitors.[11] Similarly, we explored the use of minocycline/tetracycline as a reversible OFF system for managing acute toxicity in the TetCAR system. This consists of a bipartite split CAR system relying on TetRB and TiP interaction. Displacement by tetracycline/minocycline of the TiP-signaling domain fusion protein from the membrane-bound CAR-TetRB portion could inhibit CAR activity in a tunable and reversible manner.[12]

However, several limitations prevent these small-molecule control systems from being readily translated into clinical products. First, the use of xenogeneic or unnatural proteins such as the bacterial TetRB[12] or the viral NS3 protease,[9] or the neoepitopes such as the LD3 and similar engineered scaffolds,[11,13] can trigger immunogenicity.[32] Second, designer small molecules such as AP1903 and AP21967 and bcl inhibitors A1331852 and A1155463 have not been granted regulatory approval, greatly hampering clinical use. Finally, in systems where approved small molecules can be used, these small molecules often have significant pharmacologic effects and toxicities (e.g., Rapamycin is a powerful immunosuppressive and is nephrotoxic). The characteristics of an ideal system include minimally immunogenic components that can be controlled by a clinically approved small molecule with little pharmacological effects.

In designing a new system from scratch, we selected minocycline as the control molecule. Minocycline has favorable properties, which include excellent biodistribution and a high absorption rate (95−100%). Serum concentrations peak at 2−3 h and range between 0.7 and 3.9 μg/mL (1.53−8.52 μM) with a 12−24 h half-life in blood.[33−35] Minocycline can cross the blood−brain barrier[36] and also has excellent tissue penetration, with high tissue/serum concentration ratios in liver and bile (>10) and moderate ratios in several other organs.[37] Notably, minocycline is pharmacologically inert apart from antibiotic properties, allowing for long-term use with a good safety profile.[38]

We first sought to isolate a camelid sdAb fragment with specificity toward minocycline. sdAbs are minimally immunogenic due to their high similarity to human VH3-23 family.[39] sdAbs are also attractive as a modular protein control system with their reduced size, enhanced thermal stability, and higher hydrophilicity, resulting in lower aggregation propensities.[40,41] The deep paratopes formed by CDR and framework regions of sdAbs, combined with conformational flexibility, enables binding to small molecules (haptens) in a highly specific fashion, with affinity ranges from pM to μM (affinity examples include PP6 dye, 2.5 nM;[42] picloram, 3−354 μM;[43] auxin, 0.5−20 μM;[44] methotrexate, 29−515 nM;[45] 15-acetyl-deoxynivalenol/15-AcDON, 5−215 μM;[46] and triclocarbon, 0.98−1.37 nM[47]) and with an ability to differentiate between similar analogues.[48,49] sdAbs have been employed in the detection of product contaminants,[49] chromatographic extraction,[50] and more recently, for remote-controlled biological functions via hapten-induced sdAb dimerization.[51]

We conjugated minocycline to KLH to improve the immunogenicity in alpaca. Further, alternating between KLH- and BSA-conjugated minocycline during sequential panning of an immune library ensured specificity toward the hapten rather than linker or carrier protein. The isolated

https://doi.org/10.1021/acschembio.3c00521
ACS Chem. Biol. 2024, 19, 308−324

aMinoC1 sdAb displayed strong specificity toward minocycline, in line with previously described antibody−hapten interactions,[45−47] and without cross-reactivity toward the close analogues doxycycline and tetracycline. Additionally, with an affinity of 31 nM, it was within the range of affinities previously described for small-molecule control systems.[11,12] Binding to minocycline also showed a substantial increase in Tm_{50} (79.5 and 89.6 °C) for the sdAb, suggesting a conformational stabilizing event occurring during binding.

We sought to develop an OFF system. Hence, we required a moiety that would compete with minocycline for sdAb binding. A cyclic 7-mer peptide format was selected as the binding partner, taking advantage of the cysteine-constrained structural integrity to elicit high-affinity interactions.[52−55] Phage display panning under stringent competitive elution with minocycline ensured that any enriched peptide sequences could be displaceable by the drug. The selected peptide demonstrated an affinity of 111 nM and could be rapidly and reversibly displaced by minocycline.

In the absence of a solved complex structure due to low-resolution crystal formation, we employed an alanine-scan approach to investigate how minocycline and the cyclic peptide interacted with sdAb. CDR3 was predominantly involved in minocycline interaction, while CDR1 and CDR2 were required for peptide engagement. This indicates that dAb interacts with distinct contact points in both cases; however, our docking simulations suggest competition for the same groove in the CDR space as the main displacement driver. Interestingly, the aMinoC1 interaction with minocycline and GWARA peptide (KD 31 nM and 111 nM, respectively) closely resembles the TetRB−tetracycline (KD 2.8 nM) and TetRB−TiP peptide (640 nM) interactions.[12,56−58]

We next explored the utility of this system to a range of potentially useful applications. We first sought to evaluate the aMinoC1 sdAb system as an OFF-switch split CAR format, showing practical clinical applications for therapeutic modulation. Our data suggested minocycline rapidly displaced the signaling domain, leading to reversible and dose-dependent CAR inhibition by 24 h using a clinically relevant dose of minocycline, which is well-tolerated in humans.[34] MinoCAR was comparable to conventional CAR T cells without significant differences in cytotoxicity or cytokine secretion in the absence of minocycline. A proof-of-concept experiment on NSG mice demonstrated efficient minocycline-mediated inhibition of functional MinoCAR T cells *in vivo* using a dosing regimen shown to result in serum concentrations lower than clinically measured levels in humans.[59] We further developed a universal CAR[60,61] (MinoUniCAR), demonstrating that the aMinoC1 sdAb/peptide interaction could be harnessed to reversibly functionalize inert CAR T cells and mediate specific antitumor activity.

To demonstrate the versatility of this system, we also explored other applications. These included an inducible OFF-switch mechanism for the constitutive signaling components. AP1097-inducible multimerization MyD88/CD40 systems have been described previously.[21,62] In contrast, our system sought to inhibit constitutive signaling of aMinoC1 and GWARA-peptide-fused MyD88/CD40 in the presence of minocycline. Our finding showed comparable levels of IFN-γ secretion to that previously described for two ON-switch MyD88/CD40 constructs,[21,62] with a dose-dependent inhibition mediated by minocycline. Controlled secretion of potent mediators, such as proinflammatory cytokines, may be desirable, especially for molecules that are characterized by safety concerns over systemic toxicity.[63] Using IL12 as an example, we demonstrated controlled secretion by exploiting the ER/Golgi retention signal peptides (KDEL).[64,65] KDEL-tagged aMinoC1 sdAb could efficiently retain IL12 (flexi-IL12) when fused to the GWARA peptide. As a final example, we demonstrated that a controllable sdAb/peptide interaction could be used to trigger tissue organization by stimulating cell−cell interactions. This system could also be adapted to build customized cell−cell communications for synthetic tissue engineering.[66]

In conclusion, we developed a novel small-molecule control system using minimally immunogenic protein domains and a widely available pharmacologically inert antibiotic as the inducer. We have demonstrated the versatility of this system by demonstrating multiple applications. Future improvements may include adapting this system to cytoplasmic applications. In this context, cysteine constraint could be substituted by two antiparallel coiled coil α-helical structures grafted with the GWARA sequence,[67] using novel linear peptides, or via the generation of a second sdAb component, similar to that described for a caffeine-induced dual sdAb dimerization for transgene expression.[68,69] However, the system in its current form may already have practical utility. Additionally, we hope that this *ab initio* approach to designing control systems around existing pharmaceuticals may be applied to the development of multiple novel orthogonal systems.

MATERIALS AND METHODS

Minocycline Conjugation. Minocycline was functionalized by the introduction of a free sulfhydryl group on a spacer arm to enable maleimide conjugation. Maleimide-activated KLH and BSA were used to conjugate the modified minocycline containing the thiol group.

Immunization Campaign. An Alpaca was immunized using minocycline conjugated to KLH. Following six subcutaneous immunizations, sera from the animal were screened to confirm seroconversion against minocycline−BSA via ELISA. Lymphocytes were collected and preserved in RNAlater for the construction of a phage display library.

Phage Display from Immunized Alpacas. Complementary DNA (cDNA) synthesis was carried out using primers designed to amplify the antibody heavy-chain-coding region (VHH) from lymphocytes extending from the variable (V) region through the constant heavy 2 domain (CH2) region. The camelid heavy chain antibody (HCAb) was isolated from classical antibody DNA by agarose gel electrophoresis and further amplified. The double-stranded DNA library was ligated into the phage display vector pHEN1 by using unique primers containing SfiI and NotI restriction sites at the 5′ and 3′ ends, respectively. The *E. coli* strain, ER2738, which has a tetracycline resistance gene linked to the F+ gene, was transformed via electroporation by incubating ER2738 electro-competent cells (Lucigen) with ligated DNA in chilled electroporation cuvettes (0.1 cm gap) prior to electroporation using the Biorad MicroPulser (EC1 cycle, time constant: 4.5−5.5 ms). An estimated library size of 5×10^8 unique clones was generated.

The library was panned against biotinylated BSA-conjugated minocycline coupled to streptavidin-coated beads at a concentration of 1 μg/mL. Minocycline−BSA-bound phages were eluted using prewarmed (37 °C) Trypsin-EDTA and rotated for 10 min at 37 °C. Two selection rounds were carried out, followed by ELISA screening, first analyzing enrichment of the polyclonal library followed by single colony selection, screening, and Sanger sequencing.

For ELISA screening, Nunc 96-well plates were coated with minocycline−BSA, minocycline−KLH, or BSA only at 1 μg/mL. Plates were blocked with 2% milk in PBS for 1 h. Whole-phage supernatant from soluble dAb and periplasmic extracted dAb was

https://doi.org/10.1021/acschembio.3c00521
ACS Chem. Biol. 2024, 19, 308−324

incubated in appropriate wells and incubated for 2 h at RT. Anti-M13-HRP (0.5 μg/mL) was added for the whole-phage ELISA and anti-Myc (0.5 μg/mL) was added for soluble protein ELISA and incubated for 1 h at RT.

Analysis of positive ELISA binding data was used to select monoclonal phages for sequencing. PCR amplification of monoclonal phage DNA was performed using a colony PCR reaction. Using the 2× Master Mix OneTaq (M0486L) protocol, PCR reactions containing 1 μL of bacteria from the phage-containing supernatant as the template DNA were set up. Amplified DNA was sequenced.

Phage Display for CX_7C Peptide Library. Cysteine-constrained 7-mer (CX_7C) peptide sequences specific to an aMino sdAb were generated using the Ph.D.-C7C Phage Display Peptide Library Kit (New England BioLabs, E8120S), a combinatorial library consisting of randomized display peptides with a disulfide-constrained loop (AC-XXXXXXX-CGGGS) fused to the pIII coat protein of the M13 phagemid. The library consists of approximately 1×10^9 unique sequences. Phagemid amplification, panning, and selection were carried out as previously described with a few methodical exceptions. Three rounds of panning and enrichment were carried out against biotinylated anti-minocycline single-domain antibody clone 1 fused to streptavidin beads. Elution of bound phagemid was carried out using 1 μM minocycline and was used directly for subsequent phagemid amplification.

Differential Scanning Fluorimetry. The Prometheus NT.48 NanoDSF instrument was used to characterize the thermal and chemical unfolding of aMinoC1 sdAb under native conditions and in the presence of minocycline. A dye-free protocol was used whereby the intrinsic fluorescence of tryptophan and tyrosine was measured by scanning samples at 330 and 350 nm to determine protein unfolding. Protein samples were normalized to 0.2−1 mg mL^{-1} and supplemented with minocycline at concentrations of 0.0001, 0.001, 0.01, 0.1, 1, 10, 100, 1000, and 2500 μM. Melting scan was carried out by setting the run at 1 °C/min temperature increments from 20 to 95 °C. Tm was calculated as first derivative of 350/330 nm ratio.

Surface Plasmon Resonance (SPR). Surface plasmon resonance (SPR) affinity and kinetic analysis were carried out using the Biacore T200 instrument (GE Healthcare). aMino sdAbs were immobilized to a CM5 sensor chip at a density of 4300−4600 RU. Binding assays were carried out using 1x HBS-EP+ running buffer. Various concentrations (2.5 μM with 2-fold serial dilutions) of the analyte were injected for 150 s at 30 μL/min with 150 s dissociation time. Glycine-HCl (pH 2.0) was used as the regeneration buffer for the sensor chips. For the rechallenge experiment, aMinoC1 was immobilized on a CM5 sensor chip and CX_7C peptide-Fc conjugates were loaded at 100 nM and injected as the analyte for 150 s at 30 μL/min. Following the injection of peptide-Fc, a small molecule at 1 μM was injected for 300 s at 30 μL/min, using dual injection function on a Biacore 8k instrument, to dissociate the peptide-Fc from the aMinoC1-peptide complex. The system was then washed using HBS-P^+ buffer for 300 s at 30 μL/min prior to rechallenge with peptide-Fc. The cycle was repeated three times following a final dissociation step of 300 s. For the alanine scanning experiments, the anti-minocycline antibody (sdAb-muIgG2a-Fc fusion) was captured on a Protein A series S sensor chip, to a density of 3000 RU. Minocycline was injected at a concentration of 5 μM with 2-fold serial dilutions, with 150 s contact time and 300 s dissociation at 30 μL/min. Glycine-HCl (pH 1.5) was used as the regeneration buffer. In each case, flow cell 1 was used for reference subtraction, and a "0 concentration" sensogram of buffer alone was used as a double reference subtraction to factor for drift. Data analysis was carried out using Biacore T200 Evaluation Software, version 3.0, and Biacore Insight evaluation software. The 1:1 Langmuir binding model was used to calculate the association (ka), dissociation (kd) rate constants, and equilibrium dissociation constant (KD).

Isothermal Titration Calorimetry (ITC). ITC measurements were performed using the PEAQ-ITC nonautomated (MicroCal) at 25 °C. The antibody sample was dialyzed overnight using 5 L of PBS (20 mM Na_3PO_4, 150 mM NaCl, pH 7.4). Minocycline (Sigma-Aldrich) was dissolved in DMSO, followed by dilution in PBS such that the final DMSO concentration was 1%. The concentration of the anti-minocycline sdAb (as murine IgG2a Fc fusion) was determined using extinction coefficients ε280 nm = 31,065 M^{-1} cm^{-1}. The sdAb-Fc antibody (2 μM) in the cell was titrated with minocycline (50 μM) using 22 injections of 10 μL made at 120 s intervals with a stirring speed of 300 rpm. The binding isotherm plot was fitted by nonlinear regression using the Origin software to a one set of sites 1:1 binding model to generate the thermodynamic parameters of the antibody−minocycline interaction.

Expression and Purification of Proteins. Antibodies were expressed by transient transfection in ExpiCHO cells as murine IgG2a Fc domain conjugates and purified using HiTrap MabSelect SuRe (GE Healthcare) affinity chromatography. Briefly, a MabSelect SuRe 1 mL column (GE Healthcare) was equilibrated with five column volumes of PBS pH 7.4 at a flow rate of 1 mL/min. The supernatant was applied to the column using the Akta Pure system at a flow rate of 1 mL/min. The column was then washed with 10 column volumes of PBS at pH 7.4 at 1 mL/min. Samples were eluted from the column using 3 mL of IgG elution buffer (Pierce, 21004) at 1 mL/min and directly loaded through a double-stacked HiTrap 5 mL desalting column. Samples were collected on a 96-well plate using a fraction collector unit at a fraction volume of 250 μL. Fractions were analyzed using SDS-PAGE to confirm the presence of an appropriate size protein band and purity of the protein sample. LCAR-B38 M antibody sequences (FDA-approved anti-BCMA CAR, Ciltacabtagene autoleucel) were obtained from patent literature.[70,71] aEGFR VHH antibody sequence was obtained from the literature.[72]

Cell Lines. HEK-293T cells (ATCC; ATCCCRL-11268) and SKOV3 cells (ATCC; ATCC HTB-77) were cultured in Iscove's modified Dulbecco's medium (IMDM) supplemented with 10% FBS (Labtech) and 2 mM GlutaMAX (Invitrogen). SupT1 cells (ECACC; 95013123) were cultured in complete RPMI (RPMI-1640, Lonza) supplemented with 10% FBS and 2 mM GlutaMAX. SupT1 cells were genetically modified by transduction with an SFG vector to express human EGFR. ExpiCHO cells were cultured in ExpiCHO medium (Gibco) using Erlenmeyer shake flasks (Corning) and maintained in a Kuhner shaker at 37 °C and 8% CO_2 at 225 rpm.

Transduction. γ-Retroviral supernatants were produced by transiently transfecting HEK-293T cells (3×10^6) with an RD114 envelope expression plasmid (a gift from M. Collins, UCL), a Gag-pol expression plasmid (a gift from E. Vanin, Baylor College of Medicine), and an SFG transgene plasmid. The transfection was carried out using GeneJuice (Millipore) in accordance with manufacturer's guidelines.

Blood was obtained from buffy coats purchased from NHSBT (NC07). PBMCs were isolated from buffy coats via density gradient sedimentation by using Ficoll. PBMCs were activated using anti-CD3 and anti-CD28 antibodies (Miltenyi Biotec). 24 h post activation, the culturing media was supplemented with 100 IU IL2 (2BScientific Limited). At 72 h, 1×10^6 PBMCs were plated on retronectin-coated 6-well plates (Takara Clonetech) with retroviral vectors and centrifuged at 1000g for 40 min. 72 h post-transduction, transduction efficiency was assessed and PBMCs were maintained in complete RPMI medium supplemented with 100 IU IL2.

Flow Cytometry. Flow cytometry was performed using the MACSQuant Analyzer 10 or MACSQuant X (Miltenyi Biotec). All flow cytometry data was analyzed using FlowJo v.7.6.2 software (Tree Star Inc., Ashland, OR). Cell staining was carried out by incubation with PBS containing the recommended concentration of antibodies at RT for 30 min. PBS washes were carried out between antibody staining. Cell viability was determined using viability dye SYTOX Blue Dead Cell Stain (ThermoFisher) prior to flow cytometric analysis. Cells were first gated for singlet population identified by FSC-H and FSC-A. Next, live cells were identified using a viability dye, followed by gating for target cell populations. The antibodies used in the study are as follows: CD3 PECy7 (Biolegend, 317334), Human CD34 APC-conjugated antibody (R&D system, FAB7227A), Human CD34 Alexa Fluor 488-conjugated antibody (R&D system, FAB7227G), Streptavidin PE (Biolegend, 405204), APC antihuman EGFR antibody (Biolegend, 352905), Alexa Fluor 488 antihuman EGFR

https://doi.org/10.1021/acschembio.3c00521
ACS Chem. Biol. 2024, 19, 308−324

antibody (Biolegend, 352907), PE anti-HA.11 Epitope Tag antibody (Biolegend, 901517), Anti-M13-HRP (Sino Biologics, 1197 mm05T-H), Anti-Myc-HRP (Genscript, A00863), and SYTOX Blue Dead Cell Stain (ThermoFisher, S10274).

FACS-Based Killing Assays. Transduced CAR T cells were determined by staining for the transduction marker RQR8 and normalized by the addition of nontransduced T cells. Effector cells were cocultured with 5.0×10^4 number of target cells (SupT1-NT, SupT1-EGFR+, SKOV3-mKate) to achieve the desired effector cell to target ratio. Where appropriate, minocycline was supplemented as a part of the culture conditions. Cocultures were incubated for 24−72 h at 37 °C and 5% CO_2. After incubation, plates were centrifuged at 400*g* for 5 min, and the supernatant containing secreted cytokines was collected for cytokine analysis. Cells were stained with anti-hCD34-APC and anti-CD3-PeCy7 to differentiate effector T cells and target cells. Cells were washed with 300 μL o PBS and stained with SYTOX Blue Dead Cell Stain dye. The percentage of target cell survival was measured relative to the number of live target cells cocultured with nonspecific CAR T cells or nontransduced PBMCs.

Reversibility and Tunability Assays. EGFR+ SKOV3-mKate cells were seeded at 1.0×10^4 cells per well in a TC-treated flat-bottomed 96-well plate. For reversibility experiments, MinoCAR ON−OFF kinetics were tested by preactivating CAR T cells by incubating cells for 2 h on plates precoated with recombinant EGFR (10 μg/mL). CAR T cells were washed using 15 mL of PBS prior to coculture. MinoCAR OFF−ON kinetics were tested by first inhibiting CAR T cells by incubating cells in RPMI supplemented with 10% FBS, 1% GlutaMAX, and 10 mM minocycline. Cells were then washed using 15 mL of PBS prior to coculture. Untreated CAR T cells were used as a control and were directly preceded to coculturing set. In each respective well, 0.5×10^4 transduced CAR T cells were cocultured with EGFR+SKOV3-mKate target cells with and without minocycline (10 μM). The Incucyte ZOOM Live-Cell Analysis System was used to carry out image capture at a rate of one image every 1 h for 150 h. Tunability experiments were carried out coculturing transduced PBMCs expressing MinoCAR and EGFR CAR (positive control) with target cells at an effector to target ratio of 1:2 and in the absence and presence of minocycline (0.625, 1.25, 2.5, 5, and 10 μM). The image capture rate of each condition was set at 1 image per hour for 72 h.

Cytokine Release Assays. IFN-γ, IL2, and IL12 secretion was measured by collecting the supernatant from the respective cell-based assay and frozen at −20 °C prior to analysis by ELISA. IFN-γ, IL2, and IL12 ELISAs were carried out using the Human IFN-γ ELISA MAX Deluxe kit, Human IL2 ELISA MAX Deluxe kit, and Human IL12 (p70) ELISA MAX Deluxe kit in accordance with the manufacturer's instructions (BioLegend).

sdAb-Peptide Cytotoxic T Cell Engager Assays. Transduced PBMCs were stained using RQR8 expression and V5 markers. Cells were then normalized to 50% efficiency by diluting with non-transduced T cells. The tumor-targeting adaptor protein (EGFR sdAb) fused to the GWARA peptide was separately expressed by CHO cell transient transfection and purified by His-tag chromatography. For the assay set up, 0.5×10^4 effector cells were cocultured with SupT1-EGFR+ target cells at a ratio of 1:2 in the presence of 15 μg/mL adaptor protein, with and without minocycline supplementation (10 μM) for 24 h. IFN-γ secretion was measured as described above.

IL12 Secretion Assays. Transduced PBMCs were stained for the independent HA expression marker by using an anti-HA-PE antibody to determine transduction efficiency. Cells were normalized to 60% using nontransduced T cells prior to assay set up. For the assay set up, 0.5×10^4 transduced cells were cultured in RPMI (RPMI-1640) supplemented with 10% fetal bovine serum (FBS), 2 mM GlutaMAX, and IL2 at a concentration of 100 UI/mL. The culture media was also supplemented with and without minocycline supplementation (0.1, 0.5, 1, and 2.5 μM). The supernatant was collected at days 1 and 7. IL12 ELISA was carried out following manufacturer's instructions (BioLegend, 431704).

Cell−Cell Binding Assays. SupT1 cells were transduced to express GWARA-CD8a spacer-CD28TM-2A-mCherry and aMinoC1 sdAb-CD8 spacer-CD28TM-2A-eGFP. 0.5×10^4 cells were cocultured in RPMI (RPMI-1640) supplemented with 10% fetal bovine serum (FBS) and 2 mM GlutaMAX. Where appropriate, the culture media was supplemented with minocycline (10 μM). Images were captured using an IncuCyte real-time imager. Time-course images were analyzed using ImageJ (NIH v1.53t) using an image analyzer (20 px^2-infinite size, 0.0−1.0 circularity).

Homology Modeling. Homology model generation and antibody−ligand docking were carried out using Schrodinger BioLuminate software. Camelid single-domain antibody templates were selected from the Protein Data Bank (PDB). An optimal template was selected as an appropriate template framework based on the composite scores, structural identities, and PDB resolutions. In total, 10 predicted CDR3 loops were generated. The quality of the homology models and amino acid backbone conformations were assessed using Ramachandran plots. The Schrodinger Protein Preparation Wizard PrimeMini Package was utilized to reduce the rigidity and optimize the homology model via energy minimization.

Alanine-scan mutagenesis of the CDR regions, as defined by the IMGT and Kabat numbering system, was carried out to generate 38 mutant anti-minocycline sdAbs-independent alanine mutations or serine mutations where alanine was substituted. Critical hotspot residues were determined using Biacore SPR binding data to determine KD values for the interaction of minocycline or ELISA binding data to determine binding to the GWARA peptide. Computational antibody−ligand docking was carried out by preparation of ligands using the Schrodinger LigPrep suite to convert 2D ligand (minocycline or GWARA) structures to produce corresponding low-energy 3D structures. A receptor grid was placed on the anti-minocycline sdAb model for ligand docking, centered on the critical residues defined by SPR and ELISA. The GlideScore function of the Schrodinger BioLuminate Glide suite was used to rank the docking models. In combination with experimental binding data from the alanine mutants, the top poses were selected for analysis.

Xenograft Model with NALM6. All animal studies were carried out in accordance with a UK Home Office-approved project license and were approved by the UCL Biological Services Ethical Review Committee. NSG mice (female, aged 6−10 weeks) were acquired from Charles River Laboratories and raised under pathogen-free conditions. On day 4, 0.5×10^6 Nalm6 cells engineered to express EGFR and HA-luciferase were injected intravenously into NSG mice. Tumor engraftment was assessed through bioluminescence imaging, employing the IVIS Spectrum system (PerkinElmer) following intraperitoneal injection of 2 mg D-luciferin. Photon emission from $EGFR^+$ NALM6-FLuc cells, expressed in photon per second per cm^2 per steradian, was quantified using Living Image software (PerkinElmer). On day 0, mice were randomly assigned to different cohorts prior to intravenous injection of 1×10^6 CAR T cells. The experiment was conducted without blinding; however, the use of bioluminescence imaging provides an objective assessment of tumor growth in this model. For mice treated with minocycline, a stock solution of 4 mg mL^{-1} minocycline hydrochloride was prepared by reconstituting minocycline hydrochloride (Sigma) in sterile PBS. Intraperitoneal injection of 100 μL (0.4 mg) was administered every 2−3 days. Mice were regularly weighed every 2 days, mice exhibiting any of weight loss exceeding 10%, signs of graft-versus-host disease, or disease progression were humanely euthanized.

Statistical Analyses. GraphPad Prism 9.0 (Graphpad Software Inc., La Jolla, CA, RRID:SCR_000306) was used to carry out statistical analyses and calculation. Specific statistical tools utilized are described in the figure legends where appropriate. Statistically significant differences were determined when the p values were <0.05. All data are presented as mean ± SD unless otherwise stated.

https://doi.org/10.1021/acschembio.3c00521
ACS Chem. Biol. 2024, 19, 308−324

■ ASSOCIATED CONTENT

Data Availability Statement

All data are available in the manuscript or the Supporting Information.

Supporting Information

The Supporting Information is available free of charge at https://pubs.acs.org/doi/10.1021/acschembio.3c00521.

Minocycline chemical conjugation (Figure S1), alpaca immunization/phage display (Figure S2), anti-minocycline sdAb SPR kinetics (Figure S3), dynamic binding of aMinoC1-Cx7C peptide−minocycline (Figure S4), minocycline ligand preparation (Figure S5), in silico immunogenicity analysis (Figure S6), EGFR+ cell lines and MinoCAR cytotoxicity (Figure S7), GWARA-EGFR sdAb adaptor dose response to UniMinoCAR (Figure S8), induced cell−cell interaction with the aMinoC1/GWARA module (Figure S9) (PDF)

Visual capture of induced cell−cell interaction with the aMinoC1/GWARA module (Supplementary Video 1) (MP4)

■ AUTHOR INFORMATION

Corresponding Author

Martin Pule − *Autolus Therapeutics, London W12 7FP, U.K.; Research Department of Haematology, UCL Cancer Institute, University College London, London WC1E 6DD, U.K.*; Email: martin.pule@ucl.ac.uk

Authors

Ram Jha − *Autolus Therapeutics, London W12 7FP, U.K.; Research Department of Haematology, UCL Cancer Institute, University College London, London WC1E 6DD, U.K.*; orcid.org/0009-0001-8015-7782

Alexander Kinna − *Autolus Therapeutics, London W12 7FP, U.K.*

Alastair Hotblack − *Research Department of Haematology, UCL Cancer Institute, University College London, London WC1E 6DD, U.K.*

Reyisa Bughda − *Autolus Therapeutics, London W12 7FP, U.K.*

Anna Bulek − *Autolus Therapeutics, London W12 7FP, U.K.*

Isaac Gannon − *Autolus Therapeutics, London W12 7FP, U.K.*

Tudor Ilca − *Autolus Therapeutics, London W12 7FP, U.K.*

Christopher Allen − *Autolus Therapeutics, London W12 7FP, U.K.*; orcid.org/0000-0002-5310-0529

Katarina Lamb − *Autolus Therapeutics, London W12 7FP, U.K.*

Abigail Dolor − *Autolus Therapeutics, London W12 7FP, U.K.*

Ian Scott − *Autolus Therapeutics, London W12 7FP, U.K.*

Farhaan Parekh − *Autolus Therapeutics, London W12 7FP, U.K.*

James Sillibourne − *Autolus Therapeutics, London W12 7FP, U.K.*; orcid.org/0000-0001-6755-3644

Shaun Cordoba − *Autolus Therapeutics, London W12 7FP, U.K.*

Shimobi Onuoha − *Autolus Therapeutics, London W12 7FP, U.K.*

Simon Thomas − *Autolus Therapeutics, London W12 7FP, U.K.*

Mathieu Ferrari − *Autolus Therapeutics, London W12 7FP, U.K.*

Complete contact information is available at: https://pubs.acs.org/10.1021/acschembio.3c00521

Funding

Autolus Ltd.

Notes

The authors declare the following competing financial interest(s): R. Jha, A. Kinna, A. Bulek, C. Allen, K. Lamb, A. Dolor, I. Scott, F. Parekh, J. Sillibourne, S. Thomas, M. Ferrari and M. Pule are employees and hold equity in Autolus Limited. R. Bughda, I. Gannon, T. Ilca, S. Cordoba and S. Onuoha are former employees and may hold equities in Autolus Limited. [§]R.J. and A.K. contributed equally. M.P. conceived the project and helped design experiments. R.J. and A.K. designed and performed experiments, data analysis, and manuscript writing. R.B., A.B., T.I., I.S., S.O., and M.F. generated and characterized binders and peptides. R.B. and I.G. performed in vitro experiments. C.A., K.L., A.D., F.P., and J.S. performed molecular cloning. A.H. performed in vivo experiments. S.T., M.F., and M.P. project supervision, data review, and manuscript writing.

Ethics declaration: R.J., A.K., A.B., C.A., K.L., A.D., I.S., F.P., J.S., S.T., M.F., and M.P. are employees and hold equity in Autolus Limited. R.B., I.G., T.I., S.C., and S.O. are former employees and may hold equities in Autolus Limited. Patent applications on the work described in this paper have or may be filed by Autolus Limited.

■ ACKNOWLEDGMENTS

Cell graphics were drawn by using pictures from Servier Medical Art. Servier Medical Art by Servier is licensed under a Creative Commons Attribution 3.0 Unported License.

■ REFERENCES

(1) Chen, J.; Zheng, X. F.; Brown, E. J.; Schreiber, S. L. Identification of an 11-KDa FKBP12-Rapamycin-Binding Domain within the 289-KDa FKBP12-Rapamycin-Associated Protein and Characterization of a Critical Serine Residue. *Proc. Natl. Acad. Sci. U.S.A.* **1995**, *92* (11), 4947−4951.

(2) Straathof, K. C.; Pulè, M. A.; Yotnda, P.; Dotti, G.; Vanin, E. F.; Brenner, M. K.; Heslop, H. E.; Spencer, D. M.; Rooney, C. M. An Inducible Caspase 9 Safety Switch for T-Cell Therapy. *Blood* **2005**, *105* (11), 4247−4254.

(3) Stavrou, M.; Philip, B.; Traynor-White, C.; Davis, C. G.; Onuoha, S.; Cordoba, S.; Thomas, S.; Pule, M. A Rapamycin-Activated Caspase 9-Based Suicide Gene. *Mol. Ther.* **2018**, *26* (5), 1266−1276.

(4) Wu, C.-Y.; Roybal, K. T.; Puchner, E. M.; Onuffer, J.; Lim, W. A. Remote Control of Therapeutic T Cells through a Small Molecule−Gated Chimeric Receptor. *Science* **2015**, *350* (6258), No. aab4077.

(5) Juillerat, A.; Marechal, A.; Filhol, J.-M.; Valton, J.; Duclert, A.; Poirot, L.; Duchateau, P. Design of Chimeric Antigen Receptors with Integrated Controllable Transient Functions. *Sci. Rep.* **2016**, *6*, No. 18950.

(6) Leung, W.-H.; Gay, J.; Martin, U.; Garrett, T. E.; Horton, H. M.; Certo, M. T.; Blazar, B. R.; Morgan, R. A.; Gregory, P. D.; Jarjour, J.; Astrakhan, A. Sensitive and Adaptable Pharmacological Control of CAR T Cells through Extracellular Receptor Dimerization. *JCI Insight* **2019**, *4* (11), No. e124430.

(7) Cook, P. J.; Yang, S. J.; Uenishi, G. I.; Grimm, A.; West, S. E.; Wang, L.-J.; Jacobs, C.; Repele, A.; Drow, T.; Boukhris, A.; Dahl, N. P.; Sommer, K.; Scharenberg, A. M.; Rawlings, D. J. A Chemically Inducible IL-2 Receptor Signaling Complex Allows for Effective in

Vitro and in Vivo Selection of Engineered CD4+ T Cells. *Mol. Ther.* **2023**, *31*, No. S1525001623002551.
(8) Brocard, J.; Warot, X.; Wendling, O.; Messaddeq, N.; Vonesch, J.-L.; Chambon, P.; Metzger, D. Spatio-Temporally Controlled Site-Specific Somatic Mutagenesis in the Mouse. *Proc. Natl. Acad. Sci. U.S.A.* **1997**, *94* (26), 14559−14563.
(9) Labanieh, L.; Majzner, R. G.; Klysz, D.; Sotillo, E.; Fisher, C. J.; Vilches-Moure, J. G.; Pacheco, K. Z. B.; Malipatlolla, M.; Xu, P.; Hui, J. H.; Murty, T.; Theruvath, J.; Mehta, N.; Yamada-Hunter, S. A.; Weber, E. W.; Heitzeneder, S.; Parker, K. R.; Satpathy, A. T.; Chang, H. Y.; Lin, M. Z.; Cochran, J. R.; Mackall, C. L. Enhanced Safety and Efficacy of Protease-Regulated CAR-T Cell Receptors. *Cell* **2022**, *185* (10), 1745−1763.e22.
(10) Li, H.-S.; Wong, N. M.; Tague, E.; Ngo, J. T.; Khalil, A. S.; Wong, W. W. High-Performance Multiplex Drug-Gated CAR Circuits. *Cancer Cell* **2022**, *40* (11), 1294−1305.e4.
(11) Giordano-Attianese, G.; Gainza, P.; Gray-Gaillard, E.; Cribioli, E.; Shui, S.; Kim, S.; Kwak, M.-J.; Vollers, S.; Osorio, A. D. J. C.; Reichenbach, P.; Bonet, J.; Oh, B.-H.; Irving, M.; Coukos, G.; Correia, B. E. A Computationally Designed Chimeric Antigen Receptor Provides a Small-Molecule Safety Switch for T-Cell Therapy. *Nat. Biotechnol.* **2020**, 426−432.
(12) Hotblack, A.; Kokalaki, E. K.; Palton, M. J.; Cheung, G. W.-K.; Williams, I. P.; Manzoor, S.; Grothier, T. I.; Piapi, A.; Fiaccadori, V.; Wawrzyniecka, P.; Roddy, H. A.; Agliardi, G.; Roddie, C.; Onuoha, S.; Thomas, S.; Cordoba, S.; Pule, M. Tunable Control of CAR T Cell Activity through Tetracycline Mediated Disruption of Protein−Protein Interaction. *Sci. Rep.* **2021**, *11* (1), No. 21902.
(13) Zajc, C. U.; Dobersberger, M.; Schaffner, I.; Mlynek, G.; Pühringer, D.; Salzer, B.; Djinović-Carugo, K.; Steinberger, P.; Linhares, A. D. S.; Yang, N. J.; Obinger, C.; Holter, W.; Traxlmayr, M. W.; Lehner, M. A Conformation-Specific ON-Switch for Controlling CAR T Cells with an Orally Available Drug. *Proc. Natl. Acad. Sci. U.S.A.* **2020**, *117* (26), 14926−14935.
(14) Clackson, T.; Yang, W.; Rozamus, L. W.; Hatada, M.; Amara, J. F.; Rollins, C. T.; Stevenson, L. F.; Magari, S. R.; Wood, S. A.; Courage, N. L.; Lu, X.; Cerasoli, F., Jr; Gilman, M.; Holt, D. A. Redesigning an FKBP-Ligand Interface to Generate Chemical Dimerizers with Novel Specificity. *Proc. Natl. Acad. Sci. U.S.A.* **1998**, *95* (18), 10437−10442.
(15) Dunbar, J.; Krawczyk, K.; Leem, J.; Marks, C.; Nowak, J.; Regep, C.; Georges, G.; Kelm, S.; Popovic, B.; Deane, C. M. SAbPred: A Structure-Based Antibody Prediction Server. *Nucleic Acids Res.* **2016**, *44* (W1), W474−W478.
(16) Gao, S. H.; Huang, K.; Tu, H.; Adler, A. S. Monoclonal Antibody Humanness Score and Its Applications. *BMC Biotechnol.* **2013**, *13* (1), 55.
(17) Sette, A.; Vitiello, A.; Reherman, B.; Fowler, P.; Nayersina, R.; Kast, W. M.; Melief, C. J.; Oseroff, C.; Yuan, L.; Ruppert, J.; Sidney, J.; Del Guercio, M. F.; Southwood, S.; Kubo, R. T.; Chesnut, R. W.; Grey, H. M.; Chisari, F. V. The Relationship between Class I Binding Affinity and Immunogenicity of Potential Cytotoxic T Cell Epitopes. *J. Immunol.* **1994**, *153* (12), 5586−5592.
(18) Calis, J. J. A.; Maybeno, M.; Greenbaum, J. A.; Weiskopf, D.; De Silva, A. D.; Sette, A.; Keşmir, C.; Peters, B. Properties of MHC Class I Presented Peptides That Enhance Immunogenicity. *PLoS Comput. Biol.* **2013**, *9* (10), No. e1003266.
(19) Zhou, S.; Liu, M.; Ren, F.; Meng, X.; Yu, J. The Landscape of Bispecific T Cell Engager in Cancer Treatment. *Biomarker Res.* **2021**, *9* (1), 38.
(20) Goebeler, M.-E.; Bargou, R. C. T Cell-Engaging Therapies — BiTEs and Beyond. *Nat. Rev. Clin. Oncol.* **2020**, *17* (7), 418−434.
(21) Foster, A. E.; Mahendravada, A.; Shinners, N. P.; Chang, W.-C.; Crisostomo, J.; Lu, A.; Khalil, M.; Morschl, E.; Shaw, J. L.; Saha, S.; Duong, M. T.; Collinson-Pautz, M. R.; Torres, D. L.; Rodriguez, T.; Pentcheva-Hoang, T.; Bayle, J. H.; Slawin, K. M.; Spencer, D. M. Regulated Expansion and Survival of Chimeric Antigen Receptor-Modified T Cells Using Small Molecule-Dependent Inducible MyD88/CD40. *Mol. Ther.* **2017**, *25* (9), 2176−2188.
(22) Koneru, M.; Purdon, T. J.; Spriggs, D.; Koneru, S.; Brentjens, R. J. IL-12 Secreting Tumor-Targeted Chimeric Antigen Receptor T Cells Eradicate Ovarian Tumors in Vivo. *Oncoimmunology* **2015**, *4* (3), No. e994446.
(23) Mackensen, A.; Müller, F.; Mougiakakos, D.; Böltz, S.; Wilhelm, A.; Aigner, M.; Völkl, S.; Simon, D.; Kleyer, A.; Munoz, L.; Kretschmann, S.; Kharboutli, S.; Gary, R.; Reimann, H.; Rösler, W.; Uderhardt, S.; Bang, H.; Herrmann, M.; Ekici, A. B.; Buettner, C.; Habenicht, K. M.; Winkler, T. H.; Krönke, G.; Schett, G. Anti-CD19 CAR T Cell Therapy for Refractory Systemic Lupus Erythematosus. *Nat. Med.* **2022**, *28*, 2124−2132.
(24) Sterner, R. C.; Sterner, R. M. CAR-T Cell Therapy: Current Limitations and Potential Strategies. *Blood Cancer J.* **2021**, *11* (4), 69.
(25) Tucci, F.; Galimberti, S.; Naldini, L.; Valsecchi, M. G.; Aiuti, A. A Systematic Review and Meta-Analysis of Gene Therapy with Hematopoietic Stem and Progenitor Cells for Monogenic Disorders. *Nat. Commun.* **2022**, *13* (1), No. 1315.
(26) Valadez-Barba, V.; Cota-Coronado, A.; Hernández-Pérez, O. R.; Lugo-Fabres, P. H.; Padilla-Camberos, E.; Díaz, N. F.; Díaz-Martínez, N. E. IPSC for Modeling Neurodegenerative Disorders. *Regener. Ther.* **2020**, *15*, 332−339.
(27) Brudno, J. N.; Kochenderfer, J. N. Recent Advances in CAR T-Cell Toxicity: Mechanisms, Manifestations and Management. *Blood Rev.* **2019**, *34*, 45−55.
(28) Banaszynski, L. A.; Liu, C. W.; Wandless, T. J. Characterization of the FKBP.Rapamycin.FRB Ternary Complex. *J. Am. Chem. Soc.* **2005**, *127* (13), 4715−4721.
(29) Muthuswamy, S. K.; Gilman, M.; Brugge, J. S. Controlled Dimerization of ErbB Receptors Provides Evidence for Differential Signaling by Homo- and Heterodimers. *Mol. Cell. Biol.* **1999**, *19* (10), 6845−6857.
(30) Heitman, J.; Movva, N. R.; Hall, M. N. Targets for Cell Cycle Arrest by the Immunosuppressant Rapamycin in Yeast. *Science* **1991**, *253* (5022), 905−909.
(31) Bayle, J. H.; Grimley, J. S.; Stankunas, K.; Gestwicki, J. E.; Wandless, T. J.; Crabtree, G. R. Rapamycin Analogs with Differential Binding Specificity Permit Orthogonal Control of Protein Activity. *Chem. Biol.* **2006**, *13* (1), 99−107.
(32) Berger, C.; Flowers, M. E.; Warren, E. H.; Riddell, S. R. Analysis of Transgene-Specific Immune Responses That Limit the in Vivo Persistence of Adoptively Transferred HSV-TK−Modified Donor T Cells after Allogeneic Hematopoietic Cell Transplantation. *Blood* **2006**, *107* (6), 2294−2302.
(33) Agwuh, K. N. Pharmacokinetics and Pharmacodynamics of the Tetracyclines Including Glycylcyclines. *J. Antimicrob. Chemother.* **2006**, *58* (2), 256−265.
(34) Garrido-Mesa, N.; Zarzuelo, A.; Gálvez, J. Minocycline: Far beyond an Antibiotic. *Br. J. Pharmacol.* **2013**, *169* (2), 337−352.
(35) Lashinsky, J. N.; Henig, O.; Pogue, J. M.; Kaye, K. S. Minocycline for the Treatment of Multidrug and Extensively Drug-Resistant A. Baumannii: A Review. *Infect. Dis. Ther.* **2017**, *6* (2), 199−211.
(36) Fagan, S. C.; Edwards, D. J.; Borlongan, C. V.; Xu, L.; Arora, A.; Feuerstein, G.; Hess, D. C. Optimal Delivery of Minocycline to the Brain: Implication for Human Studies of Acute Neuroprotection. *Exp. Neurol.* **2004**, *186* (2), 248−251.
(37) Carney, S.; Butcher, R. A.; Dawborn, J. K.; Pattison, G. Minocycline Excretion and Distribution in Relation to Renal Function in Man. *Clin. Exp. Pharmacol. Physiol.* **1974**, *1* (4), 299−308.
(38) Goulden, V.; Glass, D.; Cunliffe, W. J. Safety of Long-Term High-Dose Minocycline in the Treatment of Acne. *Br. J. Dermatol.* **1996**, *134* (4), 693−695.
(39) Klarenbeek, A.; Mazouari, K. E.; Desmyter, A.; Blanchetot, C.; Hultberg, A.; de Jonge, N.; Roovers, R. C.; Cambillau, C.; Spinelli, S.; Del-Favero, J.; Verrips, T.; de Haard, H. J.; Achour, I. Camelid Ig V Genes Reveal Significant Human Homology Not Seen in Therapeutic Target Genes, Providing for a Powerful Therapeutic Antibody Platform. *MAbs* **2015**, *7* (4), 693−706.

https://doi.org/10.1021/acschembio.3c00521
ACS Chem. Biol. 2024, 19, 308−324

(40) Akazawa-Ogawa, Y.; Takashima, M.; Lee, Y.-H.; Ikegami, T.; Goto, Y.; Uegaki, K.; Hagihara, Y. Heat-Induced Irreversible Denaturation of the Camelid Single Domain VHH Antibody Is Governed by Chemical Modifications. *J. Biol. Chem.* **2014**, *289* (22), 15666−15679.
(41) Ewert, S.; Cambillau, C.; Conrath, K.; Plückthun, A. Biophysical Properties of Camelid V(HH) Domains Compared to Those of Human V(H)3 Domains. *Biochemistry* **2002**, *41* (11), 3628−3636.
(42) Dumoulin, M.; Conrath, K.; Van Meirhaeghe, A.; Meersman, F.; Heremans, K.; Frenken, L. G. J.; Muyldermans, S.; Wyns, L.; Matagne, A. Single-Domain Antibody Fragments with High Conformational Stability. *Protein Sci.* **2002**, *11* (3), 500−515.
(43) Yau, K. Y. F.; Groves, M. A. T.; Li, S.; Sheedy, C.; Lee, H.; Tanha, J.; MacKenzie, C. R.; Jermutus, L.; Hall, J. C. Selection of Hapten-Specific Single-Domain Antibodies from a Non-Immunized Llama Ribosome Display Library. *J. Immunol. Methods* **2003**, *281* (1), 161−175.
(44) Sheedy, C.; Yau, K. Y. F.; Hirama, T.; MacKenzie, C. R.; Hall, J. C. Selection, Characterization, and CDR Shuffling of Naive Llama Single-Domain Antibodies Selected against Auxin and Their Cross-Reactivity with Auxinic Herbicides from Four Chemical Families. *J. Agric. Food Chem.* **2006**, *54* (10), 3668−3678.
(45) Alvarez-Rueda, N.; Behar, G.; Ferré, V.; Pugnière, M.; Roquet, F.; Gastinel, L.; Jacquot, C.; Aubry, J.; Baty, D.; Barbet, J.; Birklé, S. Generation of Llama Single-Domain Antibodies against Methotrexate, a Prototypical Hapten. *Mol. Immunol.* **2007**, *44* (7), 1680−1690.
(46) Doyle, P. J.; Arbabi-Ghahroudi, M.; Gaudette, N.; Furzer, G.; Savard, M. E.; Gleddie, S.; McLean, M. D.; Mackenzie, C. R.; Hall, J. C. Cloning, Expression, and Characterization of a Single-Domain Antibody Fragment with Affinity for 15-Acetyl-Deoxynivalenol. *Mol. Immunol.* **2008**, *45* (14), 3703−3713.
(47) Tabares-da Rosa, S.; Rossotti, M.; Carleiza, C.; Carrión, F.; Pritsch, O.; Ahn, K. C.; Last, J. A.; Hammock, B. D.; González-Sapienza, G. Competitive Selection from Single Domain Antibody Libraries Allows Isolation of High-Affinity Antihapten Antibodies That Are Not Favored in the Llama Immune Response. *Anal. Chem.* **2011**, *83* (18), 7213−7220.
(48) Ding, L.; Wang, Z.; Zhong, P.; Jiang, H.; Zhao, Z.; Zhang, Y.; Ren, Z.; Ding, Y. Structural Insights into the Mechanism of Single Domain VHH Antibody Binding to Cortisol. *FEBS Lett.* **2019**, *593*, 1873−3468.13398.
(49) Swofford, C. A.; Nordeen, S. A.; Chen, L.; Desai, M. M.; Chen, J.; Springs, S. L.; Schwartz, T. U.; Sinskey, A. J. Structure and Specificity of an ANTI-CHLORAMPHENICOL Single Domain Antibody for Detection of Amphenicol Residues. *Protein Sci.* **2022**, *31* (11), No. e4457.
(50) Franco, E. J.; Sonneson, G. J.; DeLegge, T. J.; Hofstetter, H.; Horn, J. R.; Hofstetter, O. Production and Characterization of a Genetically Engineered Anti-Caffeine Camelid Antibody and Its Use in Immunoaffinity Chromatography. *J. Chromatogr. B* **2010**, *878* (2), 177−186.
(51) Bojar, D.; Fuhrer, T.; Fussenegger, M. Purity by Design: Reducing Impurities in Bioproduction by Stimulus-Controlled Global Translational Downregulation of Non-Product Proteins. *Metab. Eng.* **2019**, *52*, 110−123.
(52) Nilsson, F.; Tarli, L.; Viti, F.; Neri, D.; Nilsson, F.; Tarli, L.; Viti, F.; Neri, D. The Use of Phage Display for the Development of Tumour Targeting Agents. Adv Drug Deliv Rev 43:165−196. *Adv. Drug Delivery Rev.* **2000**, *43*, 165−196.
(53) Aina, O. H.; Sroka, T. C.; Chen, M.-L.; Lam, K. S. Therapeutic Cancer Targeting Peptides. *Biopolymers* **2002**, *66* (3), 184−199.
(54) Joo, S. H. Cyclic Peptides as Therapeutic Agents and Biochemical Tools. *Biomol. Ther.* **2012**, *20* (1), 19−26.
(55) Krumpe, L. R. H.; Mori, T. The Use of Phage-Displayed Peptide Libraries to Develop Tumor-Targeting Drugs. *Int. J. Pept Res. Ther.* **2006**, *12* (1), 79−91.
(56) Klotzsche, M.; Berens, C.; Hillen, W. A Peptide Triggers Allostery in Tet Repressor by Binding to a Unique Site. *J. Biol. Chem.* **2005**, *280* (26), 24591−24599.
(57) Takahashi, M.; Altschmied, L.; Hillen, W. Kinetic and Equilibrium Characterization of the Tet Repressor-Tetracycline Complex by Fluorescence Measurements. Evidence for Divalent Metal Ion Requirement and Energy Transfer. *J. Mol. Biol.* **1986**, *187* (3), 341−348.
(58) Klotzsche, M.; Goeke, D.; Berens, C.; Hillen, W. Efficient and Exclusive Induction of Tet Repressor by the Oligopeptide Tip Results from Co-Variation of Their Interaction Site. *Nucleic Acids Res.* **2007**, *35* (12), 3945−3952.
(59) Zhou, J.; Ledesma, K. R.; Chang, K.-T.; Abodakpi, H.; Gao, S.; Tam, V. H. Pharmacokinetics and Pharmacodynamics of Minocycline against Acinetobacter Baumannii in a Neutropenic Murine Pneumonia Model. *Antimicrob. Agents Chemother.* **2017**, *61* (5), 10-1128.
(60) Bachmann, M.; Ehninger, A. Universal Chimeric Antigen Receptor Expressing Immune Cells for Targeting of Diverse Multiple Antigens and Method of Manufacturing the Same and Use of the Same for Treatment of Cancer, Infections and Autoimmune Disorders. WO2016030414(A2016.
(61) Cho, J. H.; Collins, J. J.; Wong, W. W. Universal Chimeric Antigen Receptors for Multiplexed and Logical Control of T Cell Responses. *Cell* **2018**, *173* (6), 1426−1438.e11.
(62) Mata, M.; Gerken, C.; Nguyen, P.; Krenciute, G.; Spencer, D. M.; Gottschalk, S. Inducible Activation of MyD88 and CD40 in CAR T Cells Results in Controllable and Potent Antitumor Activity in Preclinical Solid Tumor Models. *Cancer Discov* **2017**, *7* (11), 1306−1319.
(63) Cohen, J. Clinical Trials: IL-12 Deaths: Explanation and a Puzzle. *Science* **1995**, *270* (5238), 908a−9908.
(64) Campana, D.; Vinanica, N.; Kamaya, T.; Png, Y.; Kamiya, T. Blockade of Cd7 Expression and Chimeric Antigen Receptors for Immunotherapy of T-Cell Malignancies. WO2018098306(A2018.
(65) Chen, D.; You, F.; Xiang, S.; Wang, Y.; Li, Y.; Meng, H.; An, G.; Zhang, T.; Li, Z.; Jiang, L.; Wu, H.; Sheng, B.; Zhang, B.; Yang, L. Chimeric Antigen Receptor T Cells Derived from CD7 Nanobody Exhibit Robust Antitumor Potential against CD7-Positive Malignancies. *Am. J. Cancer Res.* **2021**, *11* (11), 5263−5281.
(66) Stevens, A. J.; Harris, A. R.; Gerdts, J.; Kim, K. H.; Trentesaux, C.; Ramirez, J. T.; McKeithan, W. L.; Fattahi, F.; Klein, O. D.; Fletcher, D. A.; Lim, W. A. Programming Multicellular Assembly with Synthetic Cell Adhesion Molecules. *Nature* **2023**, *614* (7946), 144−152.
(67) Oakley, M. G.; Kim, P. S. A Buried Polar Interaction Can Direct the Relative Orientation of Helices in a Coiled Coil †. *Biochemistry* **1998**, *37* (36), 12603−12610.
(68) Lesne, J.; Chang, H.-J.; De Visch, A.; Paloni, M.; Barthe, P.; Guichou, J.-F.; Mayonove, P.; Barducci, A.; Labesse, G.; Bonnet, J.; Cohen-Gonsaud, M. Structural Basis for Chemically-Induced Homodimerization of a Single Domain Antibody. *Sci. Rep.* **2019**, *9* (1), No. 1840.
(69) Bojar, D.; Scheller, L.; Hamri, G. C.-E.; Xie, M.; Fussenegger, M. Caffeine-Inducible Gene Switches Controlling Experimental Diabetes. *Nat. Commun.* **2018**, *9* (1), No. 2318.
(70) Zudaire Ubani, E. Bcma-Targeted Car-t Cell Therapy of Multiple Myeloma. US20210128618A12021.
(71) Fan, X.; Zhuang, Q.; Wang, P.; Wang, L.; Yang, L.; HAO, J.; Zhao, D.; He, X. Chimeric Antigen Receptors Targeting Bcma and Methods of Use Thereof. WO2018028647A12018.
(72) Roovers, R. C.; Vosjan, M. J. W. D.; Laeremans, T.; el Khoulati, R.; de Bruin, R. C. G.; Ferguson, K. M.; Verkleij, A. J.; van Dongen, G. A. M. S.; van Bergen en Henegouwen, P. M. P. A Biparatopic Anti-EGFR Nanobody Efficiently Inhibits Solid Tumour Growth. *Int. J. Cancer* **2011**, *129* (8), 2013−2024.
(73) Berdeja, J. G.; Madduri, D.; Usmani, S. Z.; Jakubowiak, A.; Agha, M.; Cohen, A. D.; Stewart, A. K.; Hari, P.; Htut, M.; Lesokhin, A.; Deol, A.; Munshi, N. C.; O'Donnell, E.; Avigan, D.; Singh, I.; Zudaire, E.; Yeh, T.-M.; Allred, A. J.; Olyslager, Y.; Banerjee, A.;

https://doi.org/10.1021/acschembio.3c00521
ACS Chem. Biol. 2024, 19, 308−324

Jackson, C. C.; Goldberg, J. D.; Schecter, J. M.; Deraedt, W.; Zhuang, S. H.; Infante, J.; Geng, D.; Wu, X.; Carrasco-Alfonso, M. J.; Akram, M.; Hossain, F.; Rizvi, S.; Fan, F.; Lin, Y.; Martin, T.; Jagannath, S. Ciltacabtagene Autoleucel, a B-Cell Maturation Antigen-Directed Chimeric Antigen Receptor T-Cell Therapy in Patients with Relapsed or Refractory Multiple Myeloma (CARTITUDE-1): A Phase 1b/2 Open-Label Study. *Lancet* **2021**, *398* (10297), 314−324.

https://doi.org/10.1021/acschembio.3c00521
ACS Chem. Biol. 2024, 19, 308−324